(Green et al., 2008), cell growth and signaling (Hooks and Cumming, 2008), and cell death (Shinzawa and Tsujimoto, 2003). In the brain of iPLA$_2\beta$-deficient mice, DHA metabolism is reduced at 4 months without overt neuropathology (Basselin et al., 2010), and an iPLA$_2\beta$ inhibitor has been reported to attenuate linoleic acid (LA) incorporation of cardiolipin (CL) in rat heart (Zachman et al., 2010). In monkey brain, iPLA$_2\beta$ is localized in axon terminals and dendritic spines of neurons (Ong et al., 2005). Although iPLA$_2\beta$ also exists in various organs (Song et al., 2010), no known non-neurological dysfunction has been reported in INAD (Gregory and Hayflick, 2008a).

Mitochondria are subcellular micro-organelles that are integral to all eukaryotic cells, being responsible for metabolic and respiratory functions. Their characteristic feature is a double-membranous architecture that separates four distinct compartments: the outer membrane, intermembrane space, inner membrane, and matrix (McBride et al., 2006). The inner membrane is highly folded into invaginations known as cristae, in which oxidative phosphorylation is catalyzed, and the phospholipids of which it is composed contain a high proportion of CL relative to that in the other membranes. The outer membrane has numerous pores for uptake and exchange of specific metabolites (McBride et al., 2006). iPLA$_2\beta$ has also been reported to exist in, and to protect, mitochondria (Seleznev et al., 2006a).

Previously, in iPLA$_2\beta$-KO mice, we demonstrated the presence of characteristic periodic acid-Schiff (PAS)-positive granules, which appeared early in apparently normal axons and later in spheroids. To clarify the pathomechanism of neuroaxonal dystrophy, we analyzed the spinal cords and sciatic nerves of iPLA$_2\beta$-KO mice, especially in the context of PAS-positive granules and spheroids. First, quantitative pathological analysis, immunohistochemistry, and ultrastructural analysis were performed, and second, imaging mass spectrometry (IMS) was performed to visualize the distribution of phospholipid in membranes.

Materials and Methods

Animals. Mice with homozygous disruption of the iPLA$_2\beta$ gene on a C57BL/6 background (Shinzawa et al., 2008), aged 15 weeks (n = 2, preclinical stage, one male and one female), 56 weeks (n = 4, early clinical stage, four females), and 95–103 weeks (n = 5, late clinical stage, two males and three females), and wild-type (WT) mice, aged 56 weeks (two males) and 95–103 weeks (one male and four females), were used. After being given an overdose of isoflurane, each animal was perfused with PBS and then 4% paraformaldehyde (PFA), followed by removal of the spinal cord and sciatic nerves. Spinal cords were immersed in the same fixative overnight at 4°C and then dehydrated and embedded in paraffin blocks. Four-micrometer-thick paraffin sections were prepared and stained with PAS. Some of the spinal cords fixed in 4% PFA were cryoprotected, and 10-μm-thick frozen sections were prepared for immunohistochemistry. Small pieces of the spinal cord and sciatic nerve were fixed with 2.5% glutaraldehyde and processed to Epon blocks as described previously (Sumi et al., 2006). Epon sections, 1 μm thick, were stained with thionin and PAS. Sciatic nerves were analyzed in transverse and longitudinal views. For analysis using liquid chromatography/electrospray ionization tandem mass spectrometry (LC/ESI-MS/MS) and imaging mass spectrometry (IMS), quickly frozen spinal cords without fixation from WT and iPLA$_2\beta$-KO mice aged 56 and 102 weeks were stored at −80°C. All animals were handled in accordance with the Guidelines for Animal Experimentation of Osaka University and those of the Japanese Government.

Immunohistochemistry. Deparaffinized sections were incubated for 30 min with 0.3% H_2O_2 to quench endogenous peroxidase activity and then washed with PBS. The primary antibodies used were a mouse monoclonal antibody against cytochrome *c* (cyt *c*) oxidase subunit I (CCO) (component of complex IV, which is the terminal enzyme in the respiratory chain on the inner membrane; 1:50; Invitrogen), a rabbit polyclonal antibody against the 20 kDa translocase of the outer mitochondrial membrane (TOM20) (one of the import receptors of mitochondrial outer membrane pores; 1:100; Dako), and a mouse monoclonal antibody against 4-hydroxy-2-nonenal (4-HNE) (an oxidized secondary product that is formed when organic lipids consisting of polyunsaturated fatty acid (PUFA) receive oxidization stress; 1:100; NOF Corporation). Autoclave treatment was performed for 9 min before incubation with the antibody against 4-HNE. Fixed frozen sections were dried and washed in PBS and incubated with a mouse monoclonal antibody against cyt *c* (1:100; BD Pharmingen). Goat anti-rabbit and anti-mouse Ig conjugated to peroxidase-labeled dextran polymer (Dako Envision+; Dako) were used as secondary antibodies. Reaction products were visualized with 3,3′-diaminobenzidine tetrahydrochloride (Vector Laboratories), and hematoxylin was used to counterstain the cell nuclei. The immunostain-

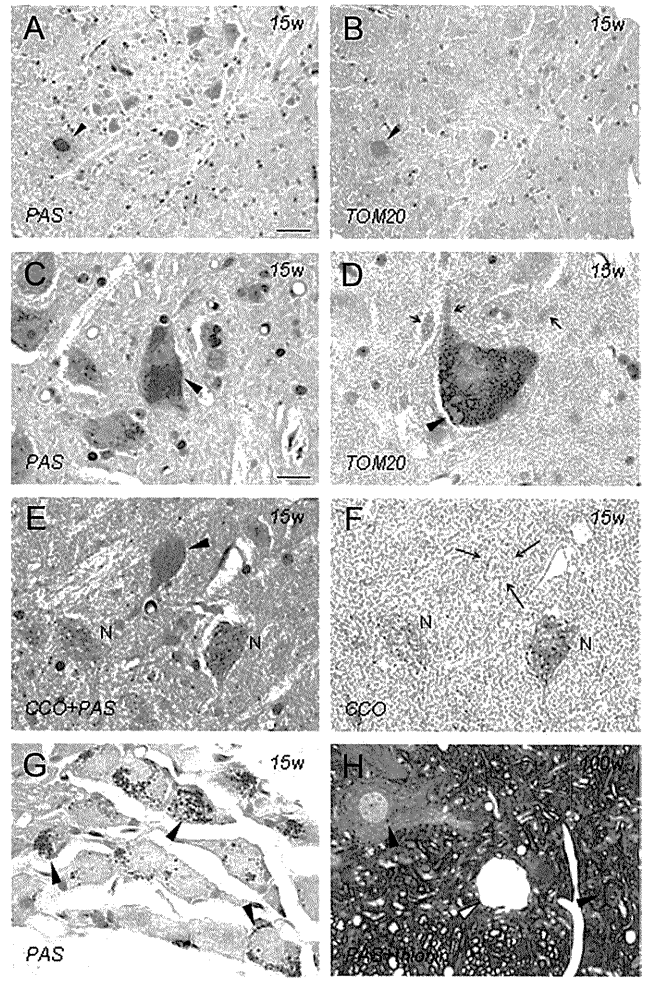

Figure 1. Immunohistochemistry of PAS-positive granules as components of mitochondrial membranes in iPLA$_2\beta$-KO mice. ***A–G***, 15 weeks; ***H***, 100 weeks; ***A–F***, ***H***, anterior horn; ***G***, dorsal root ganglia; ***A***, ***C***, ***G***, PAS staining; ***B***, ***D***, immunohistochemistry for TOM20; ***E***, double staining with PAS and immunohistochemistry for CCO; ***F***, immunohistochemistry for CCO; ***H***, double staining with PAS and thionin. ***A*** and ***B*** are serial sections, and ***E*** and ***F*** are the same section. ***A***, ***B***, A strongly PAS-positive anterior horn cell (arrowhead in ***A***) shows strong positivity for TOM20 (arrowhead in ***B***). ***C***, An anterior horn cell (arrowhead) is filled with PAS-positive granules. Apparently normal anterior horn cells also contain some PAS-positive granules. ***D***, There are many vesicles whose rims are positive for TOM20 (arrowhead) in the anterior horn cell and in neurites (arrows). ***E***, ***F***, An anterior horn cell (arrowhead in ***E***) filled with PAS-positive granules is almost negative for CCO (arrows in ***F***). The cytoplasm of other anterior horn cells (N), which contain a few PAS-positive granules, is stained for CCO. ***G***, There are many PAS-positive granules in the cytoplasm of dorsal root ganglion cells (arrowheads). ***H***, PAS-positive granules are evident in the perinuclear space of anterior horn cells and myelinated axons (arrowheads). A large vacuole (white arrowhead) is present in the neuropil. Scale bars: (in ***A***) ***A***, ***B***, 40 μm; (in ***C***) ***C–H***, 20 μm.

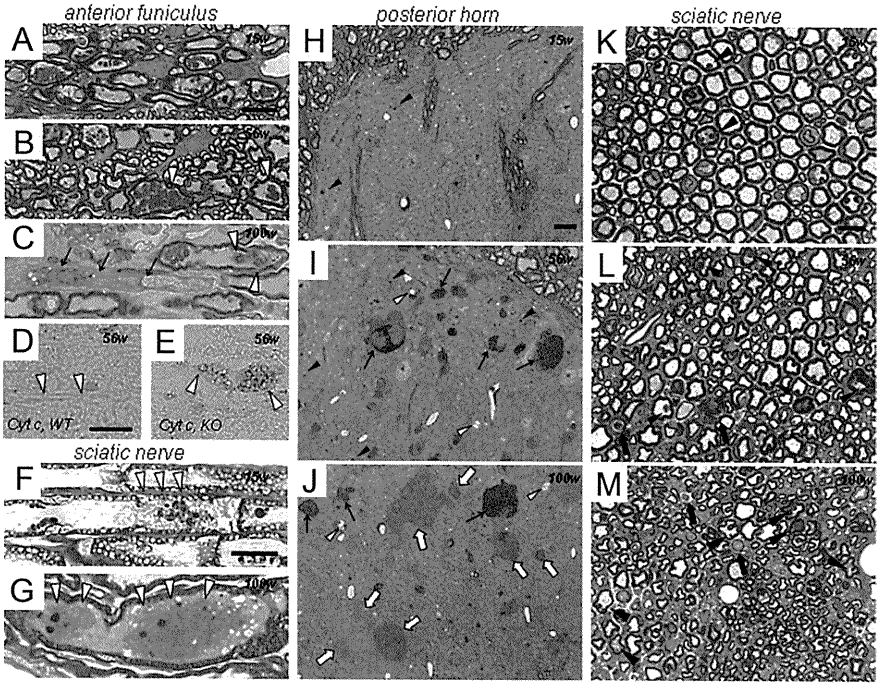

Figure 2. PAS-positive granules in proximal and distal parts of axons in iPLA$_2\beta$-KO mice. ***A***, ***F***, ***H***, ***K***, 15 weeks; ***B***, ***D***, ***E***, ***I***, ***L***, 56 weeks; ***C***, ***G***, ***J***, ***M***, 100 weeks. ***A–E***, Anterior funiculus; ***F***, ***G***, ***K–M***, sciatic nerve; ***H–J***, posterior horn. Semithin Epon sections stained with PAS and thionin (***A–C***, ***F–M***) and frozen sections immunostained for cyt *c* (***D***, ***E***). ***A***, Strongly PAS-positive granules are evident in proximal axons. ***B***, Large PAS-positive granules are frequently present in swollen axons (white arrowheads). ***C***, Degeneration of a proximal axon (arrows), with PAS-positive granules still evident in remaining axons. Some of these granules are irregular in shape and color (white arrowheads). ***D***, ***E***, Many vesicles strongly immunopositive for cyt *c* (white arrowheads) are evident in the proximal axons in iPLA$_2\beta$-KO mice (***E***) but are not observed in WT mice (white arrowheads in ***D***). ***F***, Focal axonal degeneration (white arrowheads) around vacuolated or irregular PAS-positive granules. ***G***, Two spheroids (white arrowheads) containing PAS-positive granules. ***H***, Only a few PAS-positive granules (arrowheads) are evident. ***I***, Large numbers of PAS-positive granules (arrowheads) and PAS-positive spheroids (arrows). Small vacuoles (white arrowheads) are also evident. ***J***, PAS-negative spheroids (white arrows) are frequent, in addition to PAS-positive spheroids (arrows). Vacuoles (white arrowheads) are larger than those at 56 weeks in ***I***. ***K***, A few large fibers contain PAS-positive granules (arrowheads) in the axon. ***L***, The number of large fibers is apparently reduced, and myelin ovoids (arrows) and dark axons are frequently evident. PAS-positive granules (arrowheads) are increased in number compared with the situation at 15 weeks (***K***). ***M***, Reduction of large fibers is severe. Myelin ovoids are present (arrows). PAS-positive granules of various sizes are evident in both large (black arrowheads) and small (red arrowheads) fibers. Scale bars: (in ***A***) ***A–C***, 10 μm; (in ***D***) ***D***, ***E***, 10 μm; (in ***F***) ***F***, ***G***, 10 μm; (in ***H***) ***H–J***, 10 μm; (in ***K***) ***K–M***, 10 μm.

ing patterns were compared with the PAS staining pattern, and some of the specimens were stained with PAS after the immunohistochemical staining procedures.

Quantitative pathological analysis. To study the distal parts of axons, 1-μm-thick transverse Epon sections of the lumbar cord and sciatic nerves of iPLA$_2\beta$-KO mice (15, 56, and 95–103 weeks), which had been stained with thionin and PAS, were examined. Video images were obtained using a digital camera connected to a microscope (oil immersion, 100× objective). In the lumbar cord, five fields (100 × 100 μm × 5) in the most posterior part of the posterior horns were examined. The numbers of PAS-positive granules, spheroids, and vacuoles exceeding 5 μm in diameter were counted in each mouse. In sciatic nerves, four fields (100 × 100 μm × 4) in the endoneurium were examined. The numbers of PAS-positive granules, myelin ovoids, and large fibers, with a diameter exceeding 7 μm, were counted in each mouse. The diameters of axons were measured with the aid of image analysis software (VH-H1A5; Keyence), and the data were compared statistically between iPLA$_2\beta$-KO mice aged 56 and 100 weeks by the Wilcoxon's rank sum test (Excel Toukei version 6.0; Esumi).

Ultrastructural analysis. Ultrathin sections of the spinal cord from iPLA$_2\beta$-KO mice aged 15, 56, and 100 weeks were cut and stained with uranyl acetate and lead citrate and examined using a transmission electron microscope (H-7650; Hitachi High-Technologies).

Liquid chromatography/electrospray ionization tandem mass spectrometry. For LC/ESI-MS/MS, spinal cord tissue blocks were collected into glass vials for lipid extraction (~10 mg for each), and total lipids were extracted by the Folch method (Folch et al., 1957). The ESI-MS/MS analysis was performed using a 4000Q-TRAP quadrupole linear ion trap hybrid mass spectrometer (Applied Biosystems/MDS Sciex) with an ACQUITY Ultra Performance Liquid Chromatography (Waters). A chromatographic method was developed using an ACQUITY UPLCTM BEH C18 column (2.1 × 50 mm inner diameter, 0.17 μm particle), fitted with an identically packed guard column (2.1 × 5 mm) (Waters). The column oven was maintained at 40°C. The following gradient elution with mobile phase A (acetonitrile/methanol/water at 19:19:2 v/v/v, containing 0.1% formic acid and 0.028% ammonium) and mobile phase B (isopropanol, 0.1% formic acid, and 0.028% ammonium) was used at a flow rate of 0.4 ml/min: 0–10 min, 5% B → 5% B; 10–15 min, 5% B → 50% B; 15–20 min, 50% B → 50% B; and 20–25 min, 5% B.

Mass spectrometry conditions. Tandem mass spectrometry analysis was performed in both positive, for phosphatidylcholines (PCs) and phosphatidylethanolamines (PEs), and negative, for CLs, electrospray ionization mode with the following settings: for PCs and PEs, ion spray voltage, 5500 V; curtain (nitrogen), 10 arbitrary units; and collision gas (nitrogen), "high." Specific detection was performed by multiple reaction monitoring (MRM) with the following settings: dwell time, 50 ms; declustering potential, 60 V; and resolutions of Q1 and Q3, "unit." For CLs, the following settings were used: ion spray voltage, −4500 V; curtain (nitrogen), 10 arbitrary units; and collision gas (nitrogen), "high." For MRM, the following settings were used: dwell time, 50 ms; declustering potential, −80 V; and resolutions of Q1 and Q3, "unit." The characteristic fragmentation patterns of individual lipid species were determined by enhanced product ion scanning. The results were expressed as logarithmic values of the detected intensity ratio (KO/WT), i.e., log(2, Intensity KO/Intensity WT).

Imaging mass spectrometry. Tissues blocks were sectioned at a thickness of 8 μm at −18°C using a cryostat (CM 3050; Leica Microsystems), as described previously (Schwartz et al., 2003; Sugiura et al., 2006). A 2,5-dihydroxybenzoic acid (DHB) solution (40 mg/ml DHB, 20 mM potassium acetate, 70% MetOH, and 0.1% trifluoroacetic acid) was used as the matrix solution for imaging of PC in positive ion detection mode (Sugiura and Setou, 2009). 9-Aminoacridine dissolved in 70% ethanol (50 mg/ml) was used for imaging of PE. For detection of PE in negative ion detection mode, before matrix application, tissue sections were washed with 50 mM ammonium formate for 30 s to remove endogenous salts. The matrix solution was sprayed over the tissue surface using a 0.2 mm caliber nozzle airbrush (Procon Boy FWA Platinum; Mr. Hobby). Matrices were applied simultaneously to the tissue sections that were to be compared, to equalize the analyte extraction and cocrystallization conditions. IMS measurements were performed using a matrix-assisted laser desorption/ionization tandem time-of-flight (MALDI TOF/TOF)-type instrument (Ultraflex 2 TOF/TOF; Bruker Daltonics) equipped with a 355-nm Nd:YAG laser and a modified laser focusing system. Signals between mass-to-charge ratio (*m/z*) of 400 and 1000 were collected. Raster scans on tissue surfaces were performed automatically using FlexControl and FlexImaging 2.0 software (Bruker Daltonics). The number of laser irradiations was 200 shots for each data point. Image reconstruction was performed using FlexImaging 2.0 software.

Results

Histochemical analysis of the spinal cord

In the spinal cord of iPLA$_2\beta$-KO mice at 15 weeks (presymptomatic stage), small PAS-positive granules, 0.5–1.5 μm in diameter, were frequently observed in the perinuclear space and proximal axons of anterior horn cells (Figs. 1*A*, *C*, 2*A*) but were rarely seen in the white matter. Most of the anterior horn cells contained several PAS-positive granules but appeared normal in shape. Some of the anterior horn cells were swollen and filled with the granules (Fig. 1*C*). Many PAS-positive granules were also observed in the cytoplasm of dorsal root ganglion cells (Fig. 1*G*). In the posterior horn, few PAS-positive granules were found (Fig. 2*H*). At 56 weeks (early clinical stage), swollen axons (spheroids) containing PAS-positive granules became frequent, and some of the PAS-positive granules were large and irregularly shaped (Fig. 2*B*). In the posterior horn, PAS-positive granules were increased in number, and spheroids filled with PAS-positive granules and small vacuoles became apparent (Fig. 2*I*). At 100 weeks (late clinical stage), large spheroids with or without PAS-positive granules and large vacuoles were frequently observed in the spinal cord (Figs. 1*H*, 2*J*). Severe degeneration of proximal axons was apparent, and many PAS-positive granules were found in remaining large fibers (Fig. 2*C*).

Histochemistry of the sciatic nerve

In transverse sections from control mice at 100 weeks, few myelin ovoids were found, and myelin of large fibers was often redundant. In iPLA$_2\beta$-KO mice at 15 weeks, myelin splitting was frequently evident, and myelin ovoids were rare. A few PAS-positive granules were observed in large fibers (Fig. 2*K*). In longitudinal sections, focal axonal degeneration was detected around the vacuolated PAS-positive granules (Fig. 2*F*). In transverse sections of iPLA$_2\beta$-KO mice at 56 weeks, large fibers were apparently decreased in number, and myelin ovoids and dark axons were evident (Fig. 2*L*). Large fibers with redundant, split, or thin myelin were frequent. PAS-positive granules were increased in both number and size. At 100 weeks, axonal degeneration had become more severe (Fig. 2*M*). PAS-positive granules were observed in both large and small fibers and also in spheroids (Fig. 2*G*). In longitudinal view, nodal demyelination was not evident in iPLA$_2\beta$-KO mice at any age.

Progressive increase of PAS-positive granules and axonal degeneration in the distal parts of axons

In both posterior horns of the lumbar cord and sciatic nerves of iPLA$_2\beta$-KO mice, the number of PAS-positive granules was very small at 15 weeks ($n = 2$), second largest at 56 weeks ($n = 4$), and largest at 100 weeks ($n = 5$), with statistical significance ($p < 0.05$, Wilcoxon's rank-sum test) (Fig. 3*A*,*D*). Spheroids in the posterior horns were significantly more frequent at 100 weeks than at 56 weeks ($p < 0.05$, Wilcoxon's rank-sum test) (Fig. 3*B*). In iPLA$_2\beta$-KO mice, there was no significant difference in the number of vacuoles in the posterior horns at 56 and 100 weeks (Fig. 3*C*). Myelin ovoids in sciatic nerves were very few at 15 weeks and were observed more frequently at 100 weeks than those at 56 weeks (Fig. 3*E*). Large fibers were apparently reduced in number at 56 and 100 weeks, and their number was significantly smaller at 100 weeks than at 56 weeks ($p < 0.05$, Wilcoxon's rank-sum test) (Fig. 3*F*).

Immunohistochemical analysis of mitochondrial markers

At 15 weeks, the cytoplasm of swollen anterior horn cells filled with PAS-positive granules (Fig. 1*A*,*C*) was strongly positive for TOM20 in serial sections (Fig. 1*B*). There were many vesicles whose rims

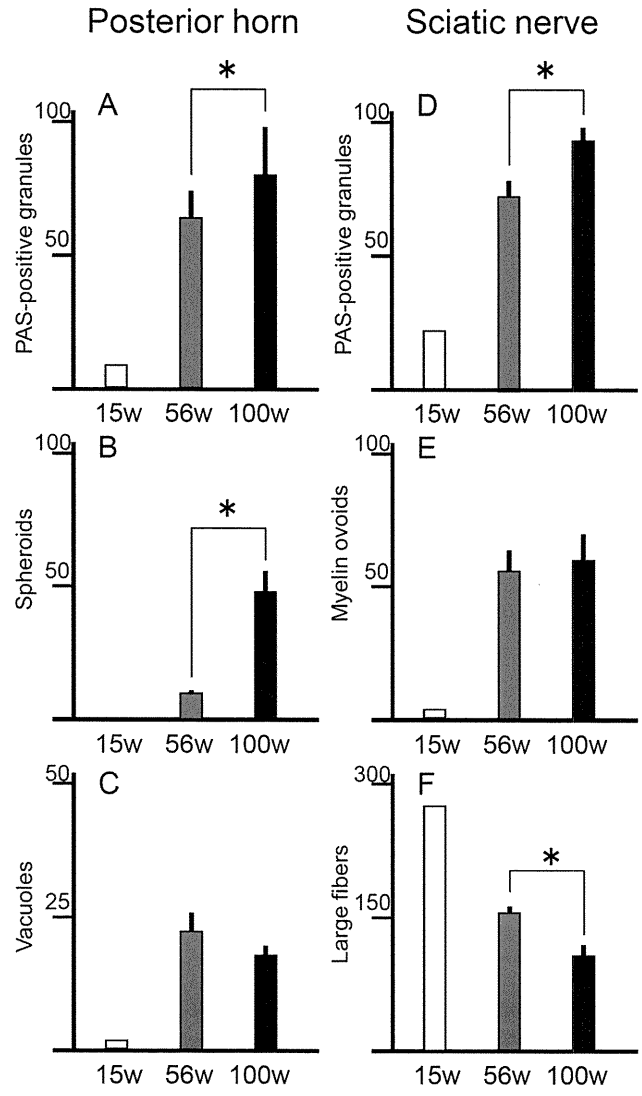

Figure 3. Progressive increase of PAS-positive granules and axonal degeneration in distal parts of axons in iPLA$_2\beta$-KO mice. ***A–C***, Posterior horns; ***D–F***, sciatic nerves. For iPLA$_2\beta$-KO mice, white bars represent data at 15 weeks ($n = 2$, mean), gray bars data at 56 weeks ($n = 4$, mean ± SD), and black bars data at 100 weeks ($n = 5$, mean ± SD). *$p < 0.05$, Wilcoxon's rank-sum test. ***A***, ***D***, In both posterior horns and sciatic nerves, PAS-positive granules are significantly more frequent at 100 weeks than at 56 weeks ($p < 0.05$, Wilcoxon's rank-sum test). ***B***, In the posterior horns, spheroids are significantly more frequent at 100 weeks than at 56 weeks ($p < 0.05$, Wilcoxon's rank-sum test). ***C***, The number of vacuoles (>5 μm) in the posterior horn of iPLA$_2\beta$-KO mice does not differ significantly between 56 and 100 weeks. ***E***, The number of myelin ovoids in sciatic nerves of iPLA$_2\beta$-KO mice does not differ significantly between 56 and 100 weeks. ***F***, Large fibers in sciatic nerves are significantly fewer at 100 weeks than at 56 weeks ($p < 0.05$, Wilcoxon's rank-sum test).

were strongly positive for TOM20 (Fig. 1*D*). PAS and immunohistochemical double staining showed that most of the PAS-positive granules in swollen anterior horn cells were strongly stained for TOM20 but negative for CCO (Fig. 1*E*,*F*). Overall, the immunoreactivities for TOM20 and CCO in the spinal cord were not apparently reduced at 15, 56, or 100 weeks (data not shown). In iPLA$_2\beta$-KO mice at 15, 56 (Fig. 2*E*), and 100 weeks, many vesicles were strongly immunopositive for cytochrome *c* in proximal axons, but no such vesicles were observed in WT mice (Fig. 2*D*).

Increase of 4-HNE in spinal cords from iPLA$_2\beta$-KO mice

The increase of 4-HNE was observed mainly in the white matter of the spinal cords of iPLA$_2\beta$-KO mice from 15 weeks (Fig. 4*C*)

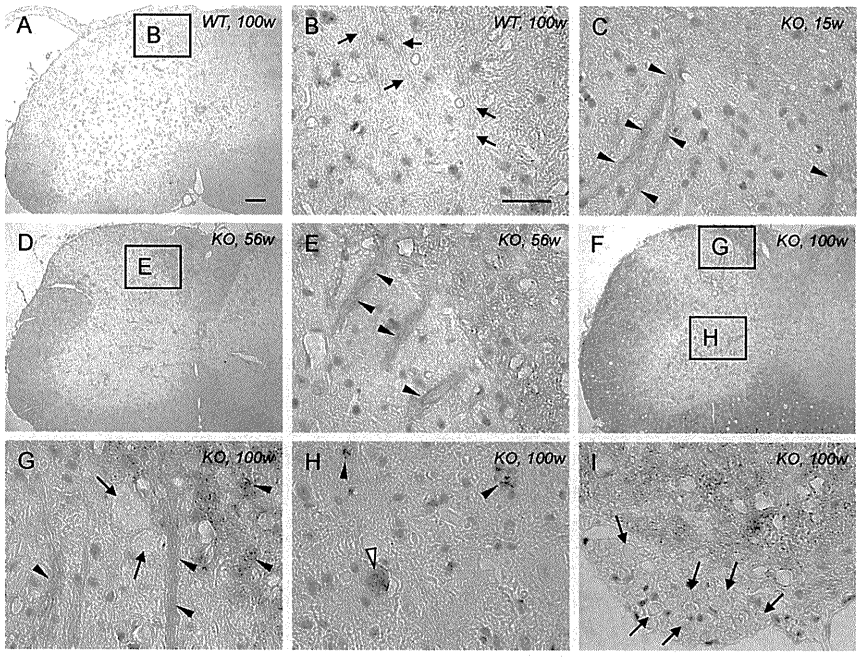

Figure 4. High expression of 4-HNE in the spinal cord of iPLA$_2\beta$-KO mice. ***A***, ***B***, WT mice at 100 weeks; ***C***, KO mice at 15 weeks; ***D***, ***E***, KO mice at 56 weeks; ***F–I***, KO mice at 100 weeks. ***A***, ***B***, No staining is evident in the control. ***B*** is a high-magnification view of the square in ***A***. Axons in the posterior horn are negative for 4-HNE (arrows). ***C***, Some of the axons are immunopositive for 4-HNE (arrowheads). ***D***, ***E***, The white matter and the axons in the posterior horn (arrowheads in ***E***) are more strongly immunopositive for 4-HNE than at 15 weeks (***C***). ***E*** is a high-magnification view of the square in ***D***. ***F–H***, The white matter is more strongly immunopositive for 4-HNE than at 56 weeks (***D***, ***E***). ***G*** and ***H*** are high-magnification views of the top and bottom squares in ***F***, respectively. The axons are strongly immunopositive for 4-HNE (arrowheads in ***G***), but large spheroids in the posterior horn are negative (arrows in ***G***). The vacuoles (arrowheads in ***H***) and the spheroid (white arrowhead in ***H***) are strongly positive for 4-HNE. ***I***, Axons in the anterior root are negative for 4-HNE (arrows). Scale bars: (in ***A***) ***A***, ***D***, ***F***, 100 μm; (in ***B***), ***C***, ***E***, ***G–I***, 10 μm.

and became prominent with age (Fig. 4*D–G*), whereas no staining was observed in WT mice (Fig. 4*A*, *B*). Some of the distal parts of axons were immunopositive for 4-HNE (Fig. 4*C*, *E*, *G*), and some spheroids and vacuoles were also immunostained in the anterior horns (Fig. 4*H*). However, most of the large spheroids in the posterior horns (Fig. 4*G*) and axons in the anterior root (Fig. 4*I*) were negative for 4-HNE. The distributions of PAS-positive granules (Fig. 1*A*, *C*, *H*, 2*A–C*, *H–J*) were not correlated with those of 4-HNE.

Ultrastructural analysis of the anterior horn and anterior funiculus

In iPLA$_2\beta$-KO mice at 15 weeks, abnormal mitochondria were frequently found in the perinuclear space of large neurons and large myelinated axons in the anterior horns (Fig. 5*A*, *B*) but were rare in the posterior horns. The cristae were partly or almost wholly diminished, and dense granules occupied the spaces created as a result (Fig. 5*A*). The structure of the cristae surrounding the granules appeared normal. Also there were many severely degenerated mitochondrion-like structures containing numerous dense granules, which were enclosed by a single membrane (Fig. 5*B*). The abnormal mitochondria were 0.5–1.5 μm in diameter and, in terms of size and distribution, appeared very similar to PAS-positive granules, which were observed microscopically after PAS staining. At 56 weeks, many dense granules were scattered around the collapsed abnormal mitochondria with degenerated cristae, and focal loss of axonal cytoskeletal elements was also evident in the vicinity (Fig. 5*C*). Another type of mitochondrial abnormality, characterized by diffusely degenerated, branching, and tubular cristae, was frequently evident (Fig. 6*A*, *B*). This type of degenerated mitochondrion was observed also in the axons of the white matter. Tubulovesicular structures, similar in size to abnormal mitochondria, were also present near them in spheroids (Fig. 6*C*). Collapse of the abnormal mitochondria without dense granules was also accompanied by focal disappearance of the axonal cytoskeleton (Fig. 6*D*). At 100 weeks, degenerated axons and abnormal mitochondria became more frequent. Some abnormal mitochondrion-like structures, with many dense granules enclosed by a single membrane, were accumulated on one side of the axon and appeared static (Fig. 5*D*). Most of the myelinated or unmyelinated spheroids were filled with tubulovesicular structures and abnormal mitochondria with degenerated inner membranes (Fig. 6*E*, *F*).

Ultrastructural analysis of the posterior horn

At 15 weeks, abnormally expanded and loose presynaptic membranes containing synaptic vesicles were observed (Fig. 7*A*). In some axon terminals, parts of the plasma membranes and synaptic vesicles had disappeared, accompanied by degenerative membranous structures and apparently normal mitochondria (Fig. 7*B*). Tubulovesicular structures sometimes followed degenerative axons of myelinated small fibers (Fig. 7*C*). After 56 weeks, vacuoles containing degenerative membranes and mitochondria were frequently evident. Irregularly shaped spheroids 3–5 μm in diameter were a common feature, and these contained various amounts of dark mitochondria, numerous dense granules, degenerative membranes, and tubulovesicular structures (Fig. 5*E*). Abnormal aggregations, which contained many dense granules of various sizes without limiting membranes, were also found in spheroids (Fig. 5*F*). Irregularly shaped and large spheroids were also evident at the ends of degenerated small fibers (Fig. 7*D*). Occasionally, large spheroids containing differing densities of tubulovesicular structures were attached to each other (Fig. 7*E*, *F*). Spheroids with a lower density of tubulovesicular structures contained degenerative axoplasm and dark mitochondria (Fig. 7*F*). Newly formed abnormal mitochondria were rare in the posterior horn.

Differences in phospholipids and fatty acids between WT and KO mice demonstrated by LC/ESI-MS/MS

Among PC species, signals for one containing DHA (16:0/22:6) and one containing AA (16:0/20:4) were prominently increased, whereas one containing oleic acid (OA) (18:0/18:1) was decreased, in the spinal cords of iPLA$_2\beta$-KO mice (Fig. 8*A*). Other PC species, such as PC (16:0/16:0), PC (16:0/16:1), PC (18:0/20:4), PC (18:0/22:6), and PC (18:1/22:6), were also increased in iPLA$_2\beta$-KO mice (Fig. 8*A*). Moreover, all five PE species analyzed, including PE (1-alkenyl-18:1/18:1), PE (1-alkenyl-18:0/18:1), PE (1-alkenyl-18:0/20:4), PE (18:0/20:4), and PE (1-alkenyl-18:0p/22:6), were increased in iPLA$_2\beta$-KO mice (Fig. 8*B*). PE (18:0/20:4) was the most heavily accumulated species in analyzed

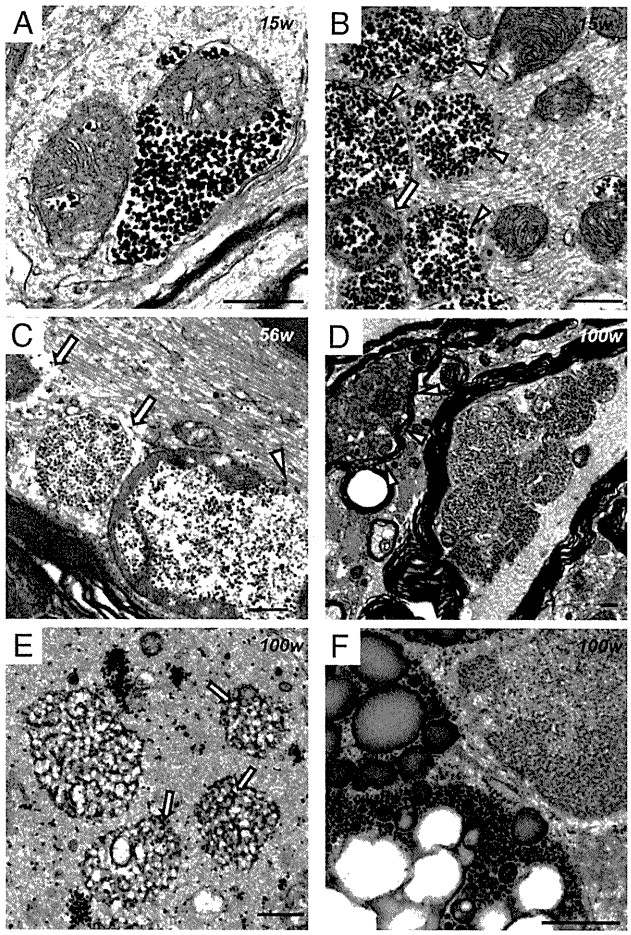

Figure 5. Electron microscopic observation of abnormal mitochondria with dense granules in iPLA$_2\beta$-KO mice. ***A***, ***B***, 15 weeks; ***C***, 56 weeks; ***D–F***, 100 weeks; ***A–D***, anterior horn; ***E***, ***F***, posterior horn. ***A***, A proportion of the mitochondrial cristae are diminished, and dense granules occupy the resulting space. The outer membrane is morphologically preserved. ***B***, An abnormal mitochondrion containing dense granules (arrow) and abnormal mitochondrion-like structures (arrowheads) with a single membrane enclosing many dense granules. Neurofilaments are mostly preserved. ***C***, Dense granules are released from abnormal mitochondria with broken membranes (white arrowhead). Focal loss of the axonal cytoskeleton is evident around abnormal mitochondria with degenerated cristae (white arrows). ***D***, Several abnormal mitochondrion-like structures have accumulated on one side of the axon. A highly degenerated axon is also evident (white arrowheads). ***E***, Dense granules are gathered or scattered in spheroids. Small and round tubulovesicular structures contain dense granules (arrows). ***F***, Spheroid containing three abnormal aggregates consisting of various-sized dense granules. The smallest one resembles an abnormal mitochondrion-like structure (***B–D***) but has no membrane around it. Scale bars, 500 nm.

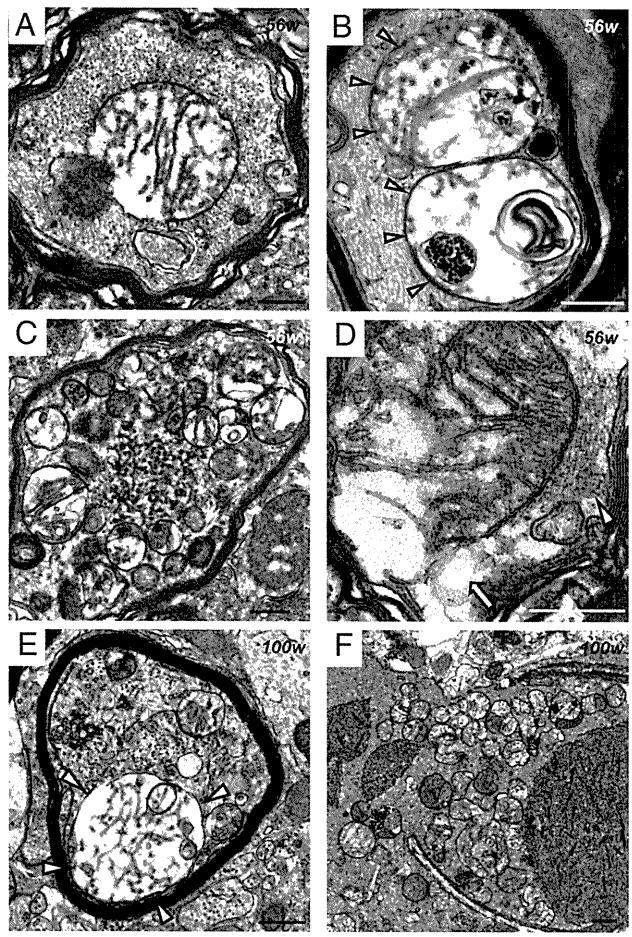

Figure 6. Abnormal mitochondria with tubular and branching cristae and tubulovesicular structures in iPLA$_2\beta$-KO mice. ***A–D***, 56 weeks; ***E***, ***F***, 100 weeks. ***A–F***, Anterior horn. ***A***, A myelinated fiber contains abnormal mitochondria, whose cristae are diffusely degenerated, tubular, and branching. Neurofilaments are mostly preserved. ***B***, Dense granules, degenerative membranes, and tubular and branching cristae are evident in the severely degenerated mitochondria (white arrowheads). ***C***, A swollen axon is filled with round tubulovesicular structures and similar-sized abnormal mitochondria. ***D***, There is focal loss (white arrow) of the axonal cytoskeleton (white arrowhead) near the broken membrane of an abnormal mitochondrion. ***E***, A myelinated axon is entirely filled with tubulovesicular structures. Abnormal mitochondria with tubular and branching cristae are also evident (white arrowheads). ***F***, Many abnormal mitochondria and various-sized round tubulovesicular structures are evident in a large spheroid. Scale bars, 500 nm.

PEs (Fig. 8*B*). Moreover, increases in the six known major molecular species of CLs (Sparagna et al., 2005) were detected in iPLA$_2\beta$-KO mice (Fig. 8*C*). Among them, CL (18:2/18:2/20:4/22:6), CL (18:0/18:2/22:6/22:6), and CL (18:2/18:2/18:2/22:6) showed large increases, and the remaining three species, CL (18:1/18:2/20:4/20:4), CL (18:1/18:2/18:2/22:6), and CL (18:2/20:4/20:4/20:4), showed mild increases (Fig. 8*C*).

IMS of the spinal cords of iPLA$_2\beta$-KO mice

By using mass spectrometry-based molecular detection, MALDI IMS can distinctly visualize the tissue distributions of various species of phospholipids that have different fatty acid compositions (Sugiura and Setou, 2009). In the positive ion mode, an ion signal at *m/z* 844 was detected and its distribution was visualized. This signal was identified as a DHA-containing PC (diacyl-16:0/22:6), which was clearly increased in the gray matter of the spinal cord of iPLA$_2\beta$-KO mice, especially in the posterior horn (Fig. 8*A-a*). IMS analyses also demonstrated an increase of PC containing AA (diacyl-16:0/20:4) in the posterior horn (Fig. 8*A-b*) and a decrease of PC containing OA (diacyl-18:0/18:1) (Fig. 8*A-c*), a component of myelin (Sugiura et al., 2009), in the white matter. In the negative ion mode, PE containing PUFAs (diacyl-18:0/20:4) was shown to be increased in the posterior horn of iPLA$_2\beta$-KO mice (Fig. 8*B-d*). These results were compatible with those of LC/ESI-MS/MS, but CLs were not detected by IMS, possibly because they were present in excessively small amounts.

Discussion

In the present study, we detected the presence of abnormal mitochondria with degenerated inner membranes from a young age in mice with KO of the group VIA phospholipase A$_2$ (iPLA$_2\beta$) gene. The collapsed and degenerated mitochondria were accompanied by focal axonal degeneration, and the plasma membranes were also

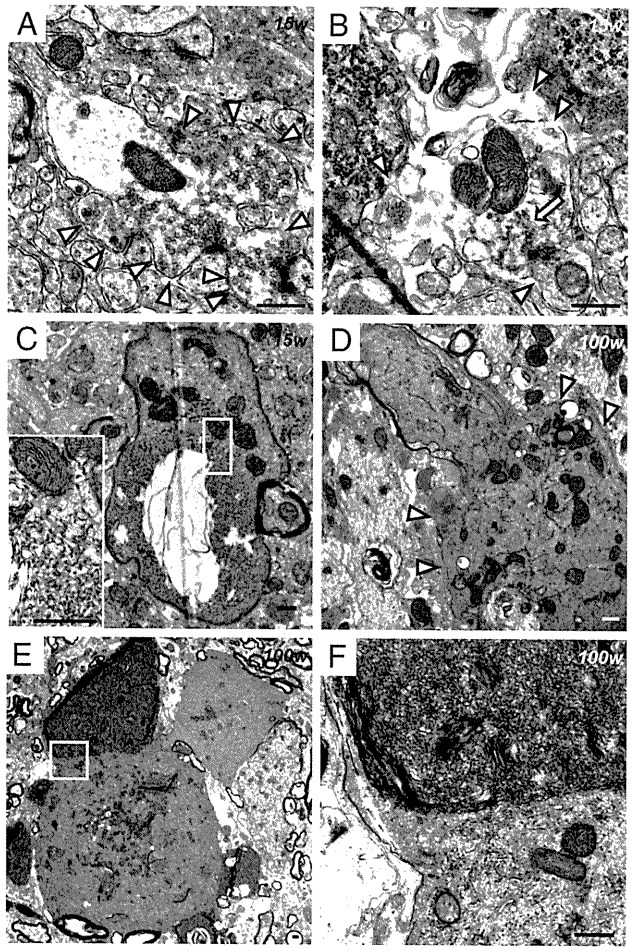

Figure 7. Electron microscopic observation of presynaptic membranes and tubulovesicular structures at the axon terminals of iPLA$_2\beta$-KO mice. ***A–C***, 15 weeks; ***D–F***, 100 weeks. ***A–F***, Posterior horn. ***A***, An abnormally expanded and loose presynaptic membrane (white arrowheads). Synaptic vesicles, apparently normal mitochondria, and postsynaptic densities are evident. ***B***, Most of the presynaptic membranes have disappeared (white arrowheads). Degenerative membranous or vesicular structures (white arrow) and apparently normal mitochondria are evident. ***C***, The tubulovesicular structures are followed by a degenerative axon containing dark mitochondria in a myelinated small fiber. The inset is a high-magnification view of the white square, which shows tubulovesicular structures and mitochondria containing dense granules. ***D***, A large and irregular spheroid (white arrowheads), containing tubulovesicular structures, degenerative membranes, and mitochondria, has formed at the axon terminal of a degenerated small fiber. ***E***, A large spheroid contains tubulovesicular structures of various densities. ***F***, High-magnification view of the white square in ***E***. Two types of tubulovesicular structures are attached to each other. The top one shows a high density of tubulovesicular structures, whereas the bottom one has a low density of tubulovesicular structures and contains mitochondria. Scale bars, 500 nm.

degenerated at the axon terminals. Thus, two kinds of degenerative membranes in axons appeared to be intrinsically associated with the pathomechanism of neuroaxonal dystrophy in iPLA$_2\beta$-KO mice.

In INAD, spheroids often contain PAS-positive granular material as well as membranous material (Cowen and Olmstead, 1963; Mahadevan et al., 2000), similar to those in iPLA$_2\beta$-KO mice. The PAS-positive granules in iPLA$_2\beta$-KO mice were identified ultrastructurally as abnormal mitochondria with degenerated inner membranes. Absence of immunoreactivity for CCO would have been attributable to degeneration of cristae, as reported previously in mice (Kirkinezos et al., 2005). Because PAS stains structures containing a high proportion of carbohydrate macromolecules and the dense granules in abnormal mitochondria resembled glycogen granules ultrastructurally, PAS staining of abnormal mitochondria might be attributable to glycosylated metabolites. Abnormal mitochondria with tubular and branching cristae, similar to those reported in INAD patients (Itoh et al., 1993; Mahadevan et al., 2000), were also observed in iPLA$_2\beta$-KO mice after 56 weeks. The difference in the structure of abnormal mitochondria might be explained by differences in the transport of metabolites attributable to membrane dysfunction (Sagun et al., 2005). Abnormal mitochondria and similar-sized tubulovesicular structures were frequently colocalized in axons, suggesting that tubulovesicular structures, a pathological hallmark of INAD, might partly originate from the abnormal mitochondria.

The vulnerability of mitochondrial inner membranes in iPLA$_2\beta$-KO mice might be attributable to rich production of reactive oxygen species (ROS) (McBride et al., 2006) and a rich content of PUFAs that can be readily peroxidized, such as LA in CL (Zhao et al., 2010). Mitochondrial inner membranes would be easily affected because of deficiency of iPLA$_2\beta$, which can hydrolyze peroxidized fatty acids to repair the membrane phospholipids oxidized by ROS, as reported previously (Zachman et al., 2010; Zhao et al., 2010). Although the evidence of lipid peroxidation in PAS-positive granules was not obtained, the increase of CL demonstrated by LC/ESI-MS/MS suggested insufficient remodeling of mitochondrial inner membranes in iPLA$_2\beta$-KO mice. Oxidation of CL leads to subsequent loss of mitochondrial membrane potential and the release of cytochrome *c* and other apoptotic proteins (Seleznev et al., 2006). In fact, liver mitochondria isolated from iPLA$_2\beta$-KO mice showed increased sensitivity to Ca^{2+} overload, resulting in easy loss of membrane potential compared with those from control mice (our unpublished data). Such mitochondrial dysfunction in the cytoplasm would finally trigger cell death as a result (Tsujimoto and Shimizu, 2007; Kagan et al., 2009). Many swollen mitochondria, which were strongly immunopositive for cytochrome *c* in the proximal axons of iPLA$_2\beta$-KO mice, might release cytochrome *c* when their membranes are broken. Ultrastructually, the axonal cytoskeleton showed focal disappearance in the proximity of collapsed abnormal mitochondria, suggesting that massive release of cytochrome *c* and other stress inducers such as ROS and lipid peroxide from the disrupted mitochondrial membranes would injure axons and impair neuronal function.

There have been no reported descriptions of non-neurological symptoms, laboratory findings, or pathological changes in internal organs in INAD (Cowen and Olmstead, 1963; Nardocci et al., 1999), although dysfunction of spermatozoa (Bao et al., 2004), a reduced insulin secretory response (Zhao et al., 2010), and acceleration of age-related changes in bone morphology (Ramanadham et al., 2008) have been reported in adult iPLA$_2\beta$-KO mice. The relatively mild phenotypes of iPLA$_2\beta$ deficiency in non-neurological tissues suggest that iPLA$_2\beta$ plays an especially important role in the nervous system, although it is widely distributed in various organs (Bao et al., 2004). Mitochondria are micro-organelles integral to all types of eukaryotic cell (McBride et al., 2006), although the lipid and protein compositions of mitochondrial membranes differ among various organs (Stepien et al., 1992). In anterior horn cells, which have marked polarity, long axons, and extensive dendritic networks (Bäumer et al., 2010), mitochondria must meet the high energy demands of neuronal function. Conversely, even in the same neuron, synaptic and nonsynaptic mitochondria differ in their functions and lipid components, the level of CL being higher in the latter than in the former (Kiebish et al., 2008). Selective degeneration of nonsynaptic mitochondria in large neurons of the spinal cord in iPLA$_2\beta$-KO mice might be associated with the individual characteristics of mitochondria unique to each functional type of cell.

Neuronal mitochondria are transported by axonal flow, connecting to kinesin motor protein with mitofustin 2 on the outer membrane (Misko et al., 2010). Because abnormal mitochondria with degenerated inner membranes were evident in the cytoplasm and proximal axons from an early stage and became significantly more frequent in the distal parts of axons later, they appeared to move to the distal portions very slowly. Prominent degeneration of axons and less marked degeneration of the neuronal cytoplasm in neuroaxonal dystrophy (Cowen and Olmstead, 1963) could be explained by the collapse of abnormal mitochondria in axons after being transported within the cell. However, apparently normal mitochondria were observed at degenerated axon terminals, suggesting that the membranes of axon terminals would also be affected by iPLA$_2\beta$ deficiency, regardless of any mitochondrial dysfunction.

iPLA$_2\beta$ shows differences in enzymatic specificity for certain fatty acids. The specific activity of iPLA$_2\beta$ with LA (18:2n-6), palmitic acid (16:0), OA (18:1n-9), and AA (20:4n-6) esterified at the *sn-2* position is 10.0, 4.3, 3.0, and 2.0 μmol · min^{-1} · mg^{-1} protein, respectively (Green et al., 2008), suggesting iPLA$_2\beta$ selectivity for LA. Conversely, the net rate of LA release from brain phospholipids, including CLs, is at least five times lower than that of DHA (22:6n-3) from PC (Green et al., 2008), suggesting the importance of iPLA$_2\beta$ for enzymatic release of DHA from PC within the brain. IMS demonstrated a prominent increase of DHA-containing PC in the gray matter, especially the posterior horn, which would have resulted from compensatory production of phospholipids in a background of membrane degeneration and lack of acyl decomposition in PC attributable to iPLA$_2\beta$ deficiency (Basselin et al., 2010). DHA is one of the important PUFAs (Green et al., 2008), possessing double- or triple-bond carbon chains and accounting for the water solubility and liquefaction of membranes (Stillwell and Wassell, 2003). Therefore, an excessive DHA content resulting from iPLA$_2\beta$ deficiency might cause abnormal expansion and degeneration of membranes. Ultrastructurally, the mitochondrial and presynaptic membranes, both of which contain PC with DHA (Omoi et al., 2006; Mitchell et al., 2007), were affected, and tubulovesicular structures were formed in the middle and ends of axons. The vulnerability of mitochondrial and presynaptic membranes might be explained by the selective localization of iPLA$_2\beta$ in mitochondria (Seleznev et al., 2006) and synapses (Ong et al., 2005).

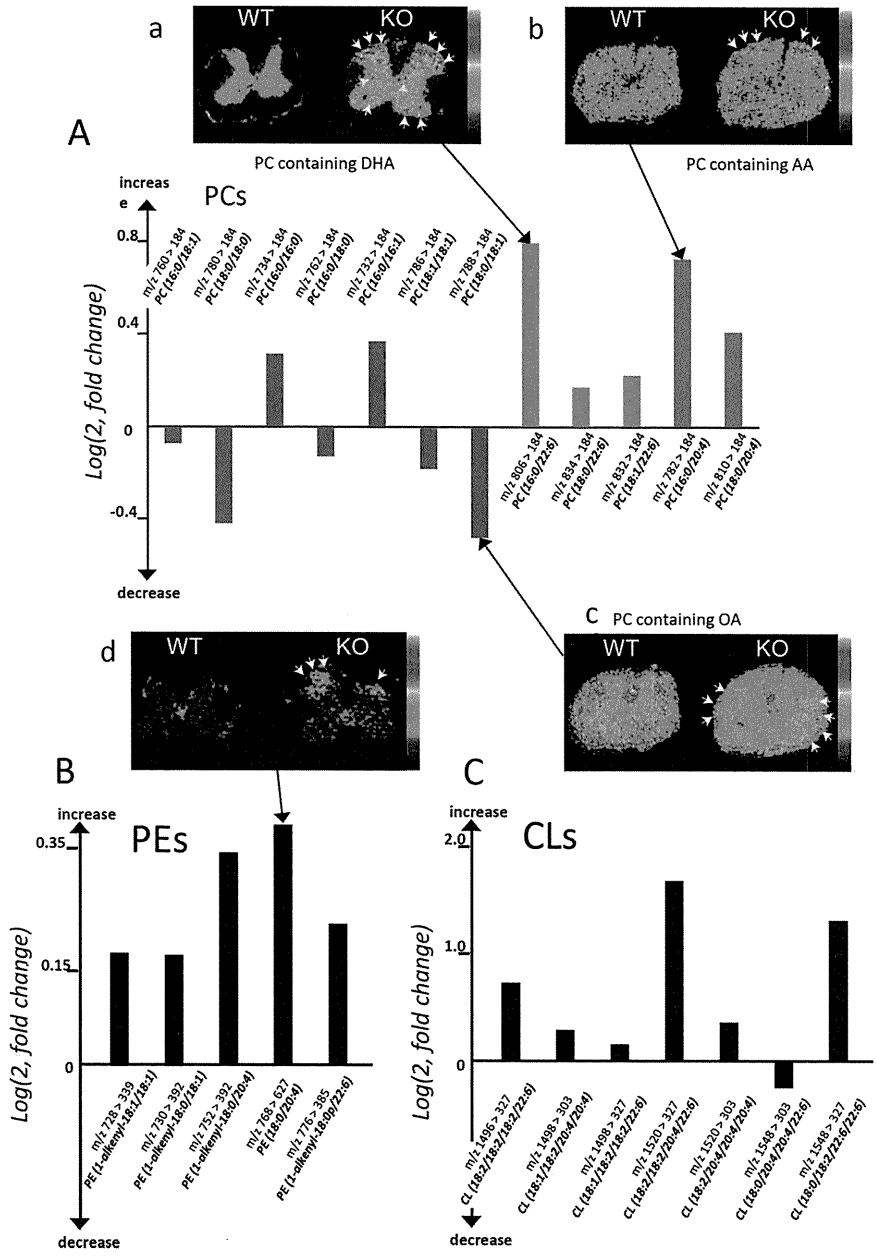

Figure 8. Quantitative lipid profiling of spinal cords from iPLA$_2\beta$-KO mice and wild-type mice. In the graphs (***A–C***), relative abundances of PCs (***A***), PEs (***B***), and CLs (***C***) in iPLA$_2\beta$-KO mice at 56 weeks, which were quantified by liquid chromatography/electrospray ionization tandem mass spectrometry in multiple reaction monitoring mode, are shown by bars, respectively. The vertical axis represents the logarithmic value of the detected intensity ratio (KO/WT), i.e., log(2, Intensity KO/Intensity WT). The bar with a positive value indicates an increase in the KO, whereas one with a negative value indicates a reduction. Blue bars represent PC species containing saturated or monounsaturated fatty acids, orange bars those containing DHA, and red bars those containing AA. In the figures (***a–d***), the distributions of lipid species that showed notable differences between KO mice and WT mice at 102 weeks are demonstrated by matrix-assisted laser desorption/ionization-imaging mass spectrometry. ***A-a***, Among PC species, one containing DHA is prominently increased in the gray matter of a KO mouse, especially in the posterior horn (arrows), compared with a WT mouse. ***A-b***, A PC species containing AA is accumulated in the posterior horn of a KO mouse (arrows). ***A-c***, A myelin constituting PC species, one containing OA, is decreased in the white matter region of a KO mouse (arrows). ***B***, All five analyzed PE species were increased in the KO spinal cord, and the most accumulated species was prominently found in the posterior horn of a KO mouse (arrows in ***d***). ***C***, Six of the seven CL molecular species analyzed were increased.

An age-dependent increase of 4-HNE was demonstrated in the axons and white matter of the spinal cord in iPLA$_2\beta$-KO mice. 4-HNE is considered to be an oxidized secondary product of lipids including CL (Liu et al., 2011) and would reflect mitochondrial dysfunction (Roede and Jones, 2010). Because CL was increased approximately threefold in iPLA$_2\beta$-KO mice and the distribution of 4-HNE was not correlated with increased PCs with

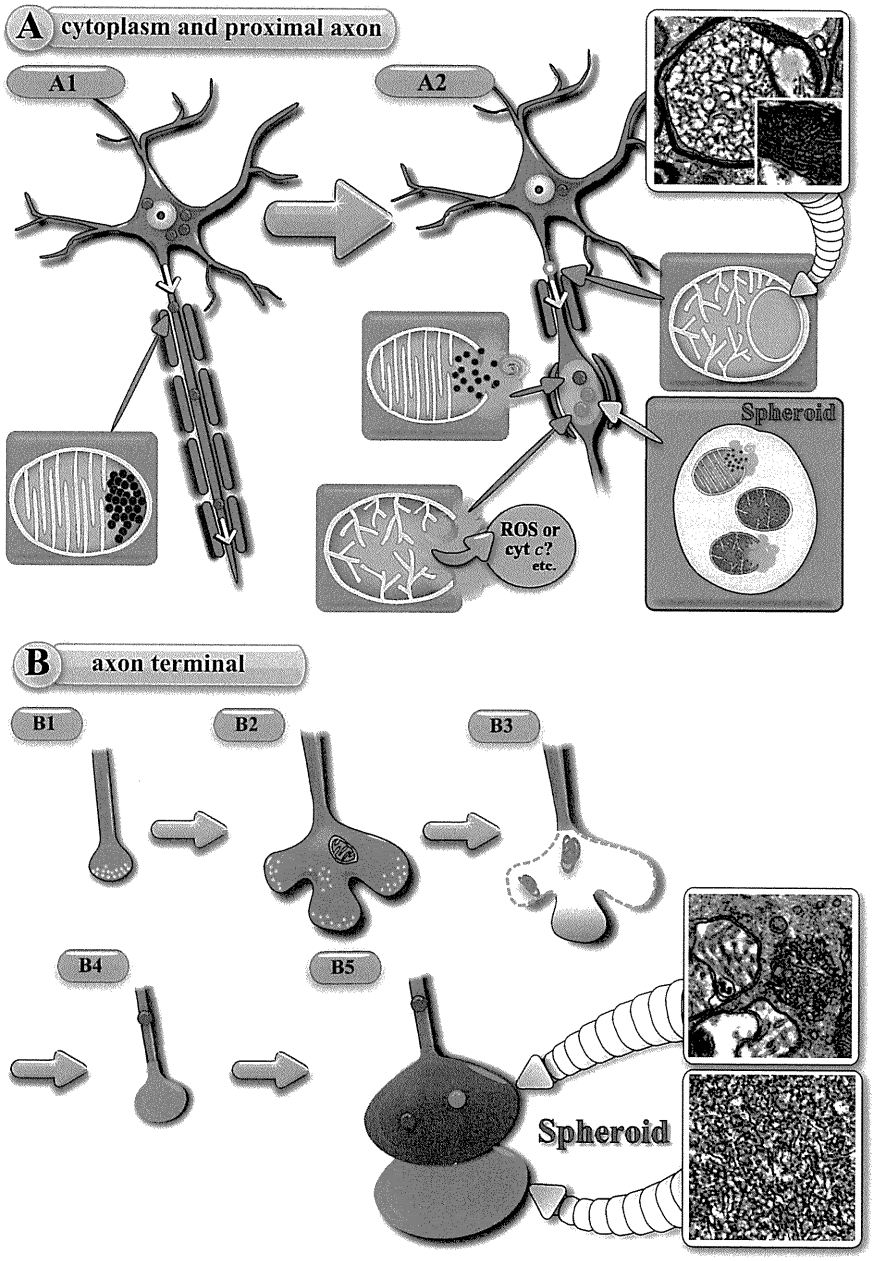

Figure 9. Schematic representation of the hypothetical pathomechanism of neuroaxonal dystrophy in iPLA$_2\beta$-KO mice. ***A***, Neuronal cytoplasm and proximal axon; ***B***, axon terminal. ***A1***, PAS-positive granules (purple color), which are indistinguishable from abnormal mitochondria, are anterogradely transported from the cytoplasm to the axon (blue color). ***A2***, When abnormal mitochondria collapse, release of cyt *c* and ROS induces spheroid formation in the middle of the axon. The photograph shows an abnormal mitochondrion containing tubulovesicular and normal cristae at 56 weeks. The square in the photo is a high-magnification view of the white square. ***B1***, Normal axon terminal with synaptic vesicles (yellow color). ***B2***, The presynaptic membrane is abnormally expanded. ***B3***, The presynaptic membrane and synaptic vesicles have disappeared, and degenerative membranes (purple color) are evident in the corresponding area. ***B4***, A spheroid (pink color) with tubulovesicular structures has formed at the axon terminal. ***B5***, Two types of tubulovesicular structures are attached to each other at the axon terminal. The distal one (pink color) shows a high density and the proximal one (blue color) a low density of tubulovesicular structures and PAS-positive granules. The photographs in the squares show two types of tubulovesicular structures observed at 100 weeks. The proximal tubulovesicular structure is followed by a swollen axon.

DHA or AA, the accumulation of 4-HNE would be related to insufficient remodeling and degeneration of the mitochondrial membrane, which was ultrastructurally prominent in axons of the white matter. The fact that the distribution of 4-HNE was inconsistent with that of PAS-positive granules, which were identical to abnormal mitochondria containing dense granules, and the distal parts of axons were positive for 4-HNE suggested that 4-HNE might be accumulated in the distal part of degenerated axons that lacked axonal flow for transport of PAS-positive granules and that 4-HNE might not be massively produced until the mitochondrial double membranes had been disrupted. The presence of 4-HNE in axons might also aggravate axonal degeneration by attacking targets within the cell and expanding into the extracellular space (Roede and Jones, 2010).

In conclusion, neuroaxonal dystrophy in iPLA$_2\beta$ deficiency is thought to be caused by two types of pathomechanism, which are associated with insufficient remodeling of the mitochondrial inner membrane and presynaptic membrane of axon terminals. The former mechanism results in insufficient remodeling of the mitochondrial inner membrane, anterograde transport (Fig. 9*A1*), and collapse of abnormal mitochondria with membrane degeneration in the middle of axons (Fig. 9*A2*). The latter mechanism results in insufficient remodeling and degeneration of presynaptic membranes at axon terminals (Fig. 9*B*). Although mitochondrial inner membranes and presynaptic membranes differ from each other, the degeneration of both finally results in the appearance of tubulovesicular structures. Spheroids containing different densities of tubulovesicular structures might originate from the two different types of membrane (Fig. 9*B4*,*B5*), i.e., those in transported mitochondria and those in presynapses. Our findings provide new insight into the pathomechanisms of neuroaxonal dystrophy in iPLA$_2\beta$ deficiency and confirm the pathological importance of tubulovesicular structures as a marker of INAD.

References

Balsinde J, Balboa MA, Dennis EA (1997) Antisense inhibition of group VI Ca^{2+}-independent phospholipase A_2 blocks phospholipid fatty acid remodeling in murine P388D1 macrophages. J Biol Chem 272:29317–29321.

Bao S, Miller DJ, Ma Z, Wohltmann M, Eng G, Ramanadham S, Moley K, Turk J (2004) Male mice that do not express group VIA phospholipase A2 produce spermatozoa with impaired motility and have greatly reduced fertility. J Biol Chem 279:38194–38200.

Basselin M, Rosa AO, Ramadan E, Cheon Y, Chang L, Chen M, Greenstein D, Wohltmann M, Turk J, Rapoport SI (2010) Imaging decreased brain docosahexaenoic acid metabolism and signaling in iPLA(2) β (VIA)-deficient mice. J Lipid Res 51:3166–3173.

Bäumer D, Ansorge O, Almeida M, Talbot K (2010) The role of RNA processing in the pathogenesis of motor neuron degeneration. Expert Rev Mol Med 12:e21.

Burke JE, Dennis EA (2009) Phospholipase A2 biochemistry. Cardiovasc Drugs Ther 23:49–59.

Cowen D, Olmstead EV (1963) Infantile neuroaxonal dystrophy. J Neuropathol Exp Neurol 22:175–236.

Engel LA, Jing Z, O'Brien DE, Sun M, Kotzbauer PT (2010) Catalytic function of PLA2G6 is impaired by mutations associated with infantile neuroaxonal dystrophy but not dystonia-parkinsonism. PLoS One 5:e12897.

Folch J, Lees M, Sloane Stanley GH (1957) A simple method for the isolation and purification of total lipides from animal tissues. J Biol Chem 226:497–509.

Green JT, Orr SK, Bazinet RP (2008) The emerging role of group VI calcium-independent phospholipase A2 in releasing docosahexaenoic acid from brain phospholipids. J Lipid Res 49:939–944.

Gregory A, Hayflick SJ (2008a) Infantile neuroaxonal dystrophy. GeneReviews. Seattle: University of Washington.

Gregory A, Westaway SK, Holm IE, Kotzbauer PT, Hogarth P, Sonek S, Coryell JC, Nguyen TM, Nardocci N, Zorzi G, Rodriguez D, Desguerre I, Bertini E, Simonati A, Levinson B, Dias C, Barbot C, Carrilho I, Santos M, Malik I, et al. (2008b) Neurodegeneration associated with genetic defects in phspholipase A_2. Neurology 71:1402–1409.

Hooks SB, Cumming BS (2008) Role of Ca^{2+}-independent phospholipase A2 in cell growth and signaling. Biochem Pharm 76:1059–1067.

Itoh K, Negishi H, Obayashi C, Hayashi Y, Hanioka K, Imai Y, Itoh H (1993) Infantile neuroaxonal dystrophy: immunohistochemical and ultrastructural studies on the central and peripheral nervous systems in infantile neuroaxonal dystrophy. Kobe J Med Sci 39:133–146.

Kagan VE, Bayir HA, Belikova NA, Kapralov O, Tyurina YY, Tyurin VA, Jiang J, Stoyanovsky DA, Wipf P, Kochanek PM, Greenberger JS, Pitt B, Shvedova AA, Borisenko G (2009) Cytochrome c/cardiolipin relations in mitochondria: a kiss of death. Free Radic Biol Med 46:1439–1453.

Khateeb S, Flusser H, Ofir R, Shelef I, Narkis G, Vardi G, Shorer Z, Levy R, Galil A, Elbedour K, Birk OS (2006) PLA2G6 mutation underlies infantile neuroaxonal dystrophy. Am J Hum Genet 79:942–948.

Kiebish MA, Han X, Cheng H, Lunceford A, Clarke CF, Moon H, Chuang JH, Seyfried TN (2008) Lipidomic analysis and electron transport chain activities in C57BL/6J mouse brain mitochondria. J Neurochem 106: 299–312.

Kirkinezos IG, Bacman SR, Hernandez D, Oca-Cossio J, Arias LJ, Perez-Pinzon MA, Bradley WG, Moraes CT (2005) Cytochrome c association with the inner mitochondrial membrane is impaired in the CNS of G93A–SOD1 mice. J Neurosci 25:164–172.

Liu W, Porter NA, Schneider C, Brash AR, Yin H (2011) Formation of 4-hydroxynonenal from cardiolipin oxidation: intramolecular peroxyl radical addition and decomposition. Free Radic Biol Med 50:166–178.

Mahadevan A, Santosh V, Gayatri N, Ratnavalli E, NandaGopal R, Vasanth A, Roy AK, Shankar SK (2000) Infantile neuroaxonal dystrophy and giant axonal neuropathy: overlap diseases of neuronal cytoskeletal elements in childhood? Clin Neuropathol 19:221–229.

Malik I, Turk J, Mancuso DJ, Montier L, Wohltmann M, Wozniak DF, Schmidt RE, Gross RW, Kotzbauer PT (2008) Disrupted membrane homeostasis and accumulation of ubiquitinated proteins in a mouse model of infantile neuroaxonal dystrophy caused by PLA2G6 mutations. Am J Pathol 172:406–416.

McBride HM, Neuspiel M, Wasiak S (2006) Mitochondria: more than just a power house. Curr Biol 16:R551–R560.

Misko A, Jiang S, Wegorzewska I, Milbrandt J, Baloh RH (2010) Mitofusin 2 is necessary for transport of axonal mitochondria and interacts with the Miro/Milton complex. J Neurosci 30:4232–4240.

Mitchell TW, Buffenstein R, Hulbert AJ (2007) Membrane phospholipid composition may contribute to exceptional longevity of the naked mole-rat (*Heterocephalus glaber*): a comparative study using shotgun lipidomics. Exp Gerontol 42:1053–1062.

Morgan NV, Westaway SK, Morton JE, Gregory A, Gissen P, Sonek S, Cangul H, Coryell J, Canham N, Nardocci N, Zorzi G, Pasha S, Rodriguez D, Desguerre I, Mubaidin A, Bertini E, Trembath RC, Simonati A, Schanen C, Johnson CA, et al. (2006) PLA_2G_6, encoding a phospholipase A_2, is mutated neurodegenerative disorders with high brain iron. Nat Genet 38:752–754.

Nardocci N, Zorzi G, Farina L, Binelli S, Scaioli W, Ciano C, Verga L, Angelini L, Savoiardo M, Bugiani O (1999) Infantile neuroaxonal dystrophy: clinical spectrum and diagnostic criteria. Neurology 52:1472–1478.

Omoi NO, Arai M, Saito M, Takatsu H, Shibata A, Fukuzawa K, Sato K, Abe K, Fukui K, Urano S (2006) Influence of oxidative stress on fusion of pre-synaptic plasma membranes of the rat brain with phosphatidyl choline liposomes, and protective effect of vitamin E. J Nutr Sci Vitaminol (Tokyo) 52:248–255.

Ong WY, Yeo JF, Ling SF, Farooqui AA (2005) Distribution of calcium-independent phospholipase A2 (iPLA 2) in monkey brain. J Neurocytol 34:447–458.

Paisan-Ruiz C, Bhatia KP, Li A, Hernandez D, Davis M, Wood NW, Hardy J, Houlden H, Singleton A, Schneider SA (2009) Characterization of PLA2G6 as a locus for dystonia-parkinsonism. Ann Neurol 65:19–23.

Ramanadham S, Yarasheski KE, Silva MJ, Wohltmann M, Novack DV, Christiansen B, Tu X, Zhang S, Lei X, Turk J (2008) Age-related changes in bone morphology are accelerated in group VIA phospholipase A2 (iPLA2beta)-null mice. Am J Pathol 172:868–881.

Roede JR, Jones DP (2010) Reactive species and mitochondrial dysfunction; mechanistic significance of 4-hydroxynonenal. Environ Mol Mutagen 51:380–390.

Sagun KC, Cárcamo JM, Golde DW (2005) Vitamin C enters mitochondria via facilitative glucose transporter 1 (Glut1) and confers mitochondrial protection against oxidative injury. FASEB J 19:1657–1667.

Schwartz SA, Reyzer ML, Caprioli RM (2003) Direct tissue analysis using matrix-assisted laser desorption/ionization mass spectrometry: practical aspects of sample preparation. J Mass Spectrom 38:699–708.

Seleznev K, Zhao C, Zhang XH, Song K, Ma ZA (2006) Calcium-independent phospholipase A2 localizes in and protects mitochondria during apoptotic induction by staurosporine. J Biol Chem 281:22275–22288.

Shinzawa K, Tsujimoto Y (2003) PLA2 activity is required for nuclear shrinkage in caspase-independent cell death. J Cell Biol 163:1219–1230.

Shinzawa K, Sumi H, Ikawa M, Matsuoka Y, Okabe M, Sakoda S, Tsujimoto Y (2008) Neuroaxonal dystrophy caused by group VIA phospholipase deficiency in mice: a model of human neurodegenerative disease. J Neurosci 28:2212–2220.

Song H, Bao S, Lei X, Jin C, Zhang S, Turk J, Ramanadham S (2010) Evidence for proteolytic processing and stimulated organelle redistribution of iPLA(2)beta. Biochim Biophys Acta 1801:547–558.

Sparagna GC, Johnson CA, McCune SA, Moore RL, Murphy RC (2005) Quantitation of cardiolipin molecular species in spontaneously hypertensive heart failure rats using electrospray ionization mass spectrometry. J Lipid Res 46:1196–1204.

Stepien G, Torroni A, Chung AB, Hodge JA, Wallace DC (1992) Differential expression of adenine nucleotide translocator isoforms in mammalian tissues and during muscle cell differentiation. J Biol Chem 267:14592–14597.

Stillwell W, Wassall SR (2003) Docosahexaenoic acid: membrane properties of a unique fatty acid. Chem Phys Lipids 126:1–27.

Strokin M, Sergeeva M, Reiser G (2003) Docosahexaenoic acid and arachidonic acid release in rat brain astrocytes is mediated by two separate isoforms of phospholipase A2 and is differently regulated by cyclic AMP and Ca^{2+}. Br J Pharmacol 139:1014–1022.

Sugiura Y, Setou M (2009) Selective imaging of positively charged polar and nonpolar lipids by optimizing matrix solution composition. Rapid Commun Mass Spectrom 23:3269–3278.

Sugiura Y, Shimma S, Setou M (2006) Thin sectioning improves the peak intensity and signal-to-noise ratio in direct tissue mass spectrometry. J Mass Spectrom Soc Jpn 54:45–48.

Sugiura Y, Konishi Y, Zaima N, Kajihara S, Nakanishi H, Taguchi R, Setou M (2009) Visualization of the cell-selective distribution of PUFA-containing phosphatidylcholines in mouse brain by imaging mass spectrometry. J Lipid Res 50:1776–1788.

Sumi H, Nagano S, Fujimura H, Kato S, Sakoda S (2006) Inverse correlation between the formation of mitochondria-derived vacuoles and Lewy-body-like hyaline inclusions in G93A superoxide-dismutase-transgenic mice. Acta Neuropathol (Berl) 112:52–63.

Tsujimoto Y, Shimizu S (2007) Role of the mitochondrial membrane permeability transition in cell death. Apoptosis 12:835–840.

Wada H, Yasuda T, Miura I, Watabe K, Sawa C, Kamijuku H, Kojo S, Taniguchi M, Nishino I, Wakana S, Yoshida H, Seino K (2009) Establishment of an improved mouse model for infantile neuroaxonal dystrophy that shows early disease onset and bears a point mutation in Pla2g6. Am J Pathol 175:2257–2263.

Zachman DK, Chicco AJ, McCune SA, Murphy RC, Moore RL, Sparagna GC (2010) The role of calcium-independent phospholipase A2 in cardiolipin remodeling in the spontaneously hypertensive heart failure rat heart. J Lipid Res 51:525–534.

Zhao Z, Zhang X, Zhao C, Choi J, Shi J, Song K, Turk J, Ma ZA (2010) Protection of pancreatic beta-cells by group VIA phospholipase A(2)-mediated repair of mitochondrial membrane peroxidation. Endocrinology 151:3038–3048.

Colocalization of 14-3-3 Proteins with SOD1 in Lewy Body-Like Hyaline Inclusions in Familial Amyotrophic Lateral Sclerosis Cases and the Animal Model

Yoko Okamoto[1☯], Yoshitomo Shirakashi[1☯], Masafumi Ihara[1]*, Makoto Urushitani[2], Miki Oono[1,2], Yasuhiro Kawamoto[1], Hirofumi Yamashita[1], Shun Shimohama[3], Shinsuke Kato[4], Asao Hirano[5], Hidekazu Tomimoto[6], Hidefumi Ito[1], Ryosuke Takahashi[1]

1 Department of Neurology, Kyoto University Graduate School of Medicine, Kyoto, Japan, **2** Molecular Neuroscience Research Center, Shiga University of Medical Science, Shiga, Japan, **3** Department of Neurology, Sapporo Medical University School of Medicine, Hokkaido, Japan, **4** Department of Neuropathology, Institute of Neurological Sciences, Faculty of Medicine, Tottori University, Tottori, Japan, **5** Division of Neuropathology, Department of Pathology, Montefiore Medical Center, New York, New York, United States of America, **6** Department of Neurology, Mie University Graduate School of Medicine, Mie, Japan

Abstract

Background and Purpose: Cu/Zn superoxide dismutase (SOD1) is a major component of Lewy body-like hyaline inclusion (LBHI) found in the postmortem tissue of SOD1-linked familial amyotrophic lateral sclerosis (FALS) patients. In our recent studies, 14-3-3 proteins have been found in the ubiquitinated inclusions inside the anterior horn cells of spinal cords with sporadic amyotrophic lateral sclerosis (ALS). To further investigate the role of 14-3-3 proteins in ALS, we performed immunohistochemical analysis of 14-3-3 proteins and compared their distributions with those of SOD1 in FALS patients and SOD1-overexpressing mice.

Methods: We examined the postmortem brains and the spinal cords of three FALS cases (A4V SOD1 mutant). Transgenic mice expressing the G93A mutant human SOD1 (mutant SOD1-Tg mice), transgenic mice expressing the wild-type human SOD1 (wild-type SOD1-Tg mice), and non-Tg wild-type mice were also subjected to the immunohistochemical analysis.

Results: In all the FALS patients, LBHIs were observed in the cytoplasm of the anterior horn cells, and these inclusions were immunopositive intensely for pan 14-3-3, 14-3-3β, and 14-3-3γ. In the mutant SOD1-Tg mice, a high degree of immunoreactivity for misfolded SOD1 (C4F6) was observed in the cytoplasm, with an even greater degree of immunoreactivity present in the cytoplasmic aggregates of the anterior horn cells in the lumbar spinal cord. Furthermore, we have found increased 14-3-3β and 14-3-3γ immunoreactivities in the mutant SOD1-Tg mice. Double immunofluorescent staining showed that C4F6 and 14-3-3 proteins were partially co-localized in the spinal cord with FALS and the mutant SOD1-Tg mice. In comparison, the wild-type SOD1-Tg and non-Tg wild-type mice showed no or faint immunoreactivity for C4F6 and 14-3-3 proteins (pan 14-3-3, 14-3-3β, and 14-3-3γ) in any neuronal compartments.

Discussion: These results suggest that 14-3-3 proteins may be associated with the formation of SOD1-containing inclusions, in FALS patients and the mutant SOD1-Tg mice.

Citation: Okamoto Y, Shirakashi Y, Ihara M, Urushitani M, Oono M, et al. (2011) Colocalization of 14-3-3 Proteins with SOD1 in Lewy Body-Like Hyaline Inclusions in Familial Amyotrophic Lateral Sclerosis Cases and the Animal Model. PLoS ONE 6(5): e20427. doi:10.1371/journal.pone.0020427

Editor: Mel B. Feany, Brigham and Women's Hospital, Harvard Medical School, United States of America

Received February 11, 2011; **Accepted** April 27, 2011; **Published** May 31, 2011

Funding: The authors have no support or funding to report.

Competing Interests: The authors have declared that no competing interests exist.

* E-mail: ihara@kuhp.kyoto-u.ac.jp

☯ These authors contributed equally to this work.

Introduction

Amyotrophic lateral sclerosis (ALS) is a fatal, progressive neurodegenerative disease characterized by the degeneration of motor neurons in the motor cortex, brainstem and spinal cord. The vast majority of ALS patients are sporadic, and approximately 5–10% of ALS cases are familial ALS (FALS) [1]. Among the FALS patients, approximately 20% are linked to mutations in the antioxidant enzyme Cu/Zn superoxide dismutase (SOD1) [2]. Mutant SOD1 proteins aggregate and form Lewy body-like hyaline inclusions (LBHIs) in the anterior horn cells of the spinal cord [3].

Transgenic mice carrying several copies of human mutant SOD1 genes show ALS-like symptoms such as progressive motor disturbances and neurogenic amyotrophy, and develop a pathology resembling ALS [4]. In brief, these Tg mice demonstrate atrophy of the motor neuronal system, vacuolar degeneration of the motor neurons, and ubiquitinated neuronal hyaline inclusions which contain SOD1 in their cell bodies and swollen processes [5].

SOD1 is a major constituent of LBHIs linked to FALS, and these LBHIs contain ubiquitin [6], phosphorylated neurofilaments [7], and a copper chaperone for superoxide dismutase [8].

The 14-3-3 proteins, a family of protein chaperones, are abundant in the brain, comprising approximately 1% of the total brain protein [9]. 14-3-3 proteins consist of seven different isoforms, named with Greek letters (β, ε, γ, η, θ, σ, and ζ). Each isoform forms homo- or hetero-dimers. 14-3-3 dimers can simultaneously bind two ligands, modulate different signaling molecules and participate in cell cycle control, cell adhesion, neuronal plasticity as well as various intracellular signal transduction pathways [10]. 14-3-3 proteins seem to control the subcellular localization of proteins and to function as adaptor molecules, stimulating protein-protein interactions. The regulation of this interaction usually involves the phosphorylation of the interacting proteins [11].

In our recent studies, several types of 14-3-3 proteins such as 14-3-3β, 14-3-3γ, 14-3-3ζ, 14-3-3θ, or 14-3-3ε have been found in the ubiquitinated inclusions of anterior horn cells from patients with sporadic ALS [12]. 14-3-3 mRNA was also demonstrated to be upregulated in the spinal cords with sporadic ALS [13].

However, the association of 14-3-3 proteins with FALS remains unknown. In this study, to investigate the role of 14-3-3 proteins and SOD1 in the pathogenesis of FALS, we performed immunohistochemical staining for 14-3-3 proteins and SOD1 in formalin-fixed, paraffin-embedded sections from patients with FALS. Transgenic mice which overexpress mutant human SOD1, transgenic mice which overexpress wild type human SOD1, and non-transgenic wild-type mice were also subjected to immunohistochemical analysis.

Methods

Ethics Statement

The protocols for genetic analysis and neuropathological procedures were approved by and performed under the guidelines of our institutional ethics committee. Informed consent was obtained from all individuals or their guardians before the analysis. The animal study was carried out in strict accordance with the guidelines for animal experimentation from the Animal Research Committee of our institution. The protocol was approved by the Animal Research Committee, Kyoto University (Permit Number: MedKyo10202).

Human FALS cases

We analyzed three cases of FALS (A4V SOD1 mutant). The clinicopathological backgrounds of these FALS cases have been previously reported [14]. These patients were members of the American "C" family. The three patients were males, and their ages at death were 39, 46 and 66 years. They were pathologically consistent with FALS with posterior column involvement [15].

Transgenic mice expressing G93A mutant human SOD1 and wild type human SOD1

We used transgenic mice expressing the G93A mutant human SOD1 gene (mutant SOD1-Tg mice) [B6SJL-TgN (SOD1-G93A) 1Gur] and wild-type human SOD1 gene (wild-type SOD1-Tg mice) [B6SJL-Tg (SOD1) 2Gur/J], which were originally obtained from the Jackson Laboratory [16]. The mutant SOD1-Tg mice develop signs of hind limb weakness at the age of 3 to 4 months. At the age of 5 to 6 months, they are not able to forage for food and water and then die. The wild-type SOD1-Tg mice show no motor symptoms [17]. We analyzed four-month-old mutant SOD1-Tg and wild-type SOD1-Tg mice (n = 4, each).

Human tissues

Human tissue blocks obtained from the different levels of spinal cords of FALS cases were embedded in paraffin. The blocks were sectioned with a microtome at 6 μm thickness for routine and immunohistochemical staining. Routine histological assessment was carried out with hematoxylin and eosin (H&E).

H&E-stained sections with LBHIs were photographed, decolorized with 70% ethanol and pretreated with 0.3% H_2O_2 in 0.1 mol/L phosphate-buffered saline (PBS) for 30 min at room temperature to inhibit any endogenous peroxidase activity. After washing with 0.1 mol/L PBS, these sections were blocked with 0.1 mol/L PBS plus 3% skim milk for 2 hours at room temperature. Then, the specimens were used for immunohistochemistry; this involved sequential incubation with primary antibody, appropriate biotinylated secondary antibody (Vector Laboratories, diluted 1:200), and avidin-biotin-peroxidase complex (ABC; Vector Laboratories, 1:200) in 0.1 mol/L PBS containing 0.3% Triton X-100 (PBST, pH 7.4). The sections were rinsed with PBST for 15 min between each step and finally visualized with 0.01% diaminobenzidinetetrahydrochloride and 0.005% H_2O_2 in 50 mmol/L Tris-HCl (pH 7.6).

Animal tissues

Mice were deeply anesthetized with sodium pentobarbital and were perfused transcardially with 0.01 mol/L PBS and then with a fixative containing 4% paraformaldehyde (PFA) and 0.2% picric acid in 0.1 mol/L phosphate buffer (PB, pH 7.4). Then, the brains and the spinal cords were removed. The tissues were post-fixed for 24 hours in 4% PFA and stored in 20% sucrose in 0.1 mol/L PB (pH 7.4). Serial lumbar spinal sections were cut into 20 μm thick sections on a cryostat, and immunohistochemical analysis was performed in the same way as human tissues described above.

Table 1. Primary antibodies.

Primary antibody				Company	Dilution
C4F6	mouse monoclonal			Reference [18]	1:1000
SOD1	goat polyclonal	C-17	SC-8637	Santa Cruz Biotechnology	1:1000
pan 14-3-3	mouse monoclonal	H-8	SC-1657	Santa Cruz Biotechnology	1:1000
14-3-3β	rabbit polyclonal	C-20	SC-628	Santa Cruz Biotechnology	1:2000
14-3-3γ	rabbit polyclonal	C-16	SC-731	Santa Cruz Biotechnology	1:2000
14-3-3ε	rabbit polyclonal	T-16	SC-1020	Santa Cruz Biotechnology	1:400
14-3-3η	goat polyclonal	E-12	SC-17287	Santa Cruz Biotechnology	1:400
14-3-3θ	rabbit polyclonal	C-17	SC-732	Santa Cruz Biotechnology	1:2000
14-3-3σ	goat polyclonal	C-18	SC-7683	Santa Cruz Biotechnology	1:400
14-3-3σ	goat polyclonal	N-14	SC-7681	Santa Cruz Biotechnology	1:400
14-3-3ζ	rabbit polyclonal	C-16	SC-1019	Santa Cruz Biotechnology	1:2000

doi:10.1371/journal.pone.0020427.t001

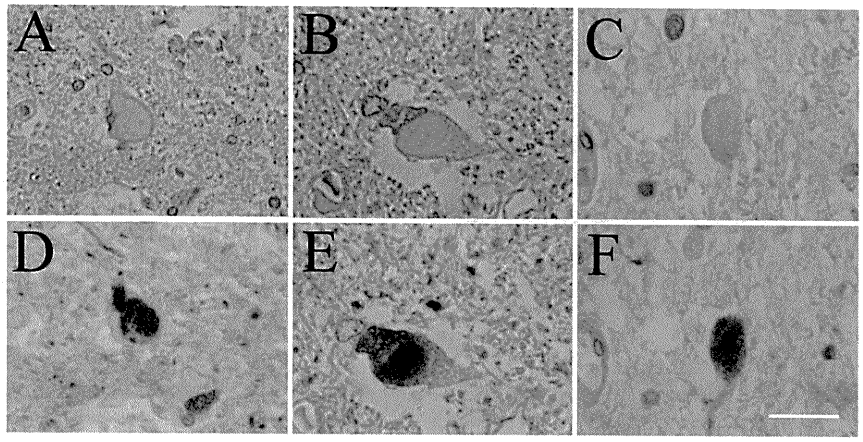

Figure 1. LBHIs immunopositive for 14-3-3 proteins in FALS patients. A, B, and C are the same sections as D, E, and F, respectively. The upper panels (A–C) are stained with H&E, and the lower panels (D–F) are immunostained with the anti-pan 14-3-3 antibody. LBHIs observed on H&E in the anterior horn cells are intensely immunopositive for pan 14-3-3. Bar indicates 100 μm in (A, D), and 50 μm in (B, C, E, F).
doi:10.1371/journal.pone.0020427.g001

Primary antibodies

As primary antibodies, we used anti-SOD1, anti-misfolded SOD1 (C4F6) [18], and anti- pan and isoform-specific 14-3-3 protein antibodies. The primary antibodies used were listed in Table 1.

Double labeling immunohistochemistry

To investigate the relationship between SOD1 and 14-3-3 proteins, spinal cord sections of the FALS cases were incubated with primary antibodies against SOD1 and pan 14-3-3, followed by incubation with FITC- or rhodamine-labeled appropriate secondary antibodies. For mouse tissues, anti-14-3-3 (β or γ) and C4F6-DyLight 488 antibodies were used. C4F6 was labeled with DyLight Fluor 488 using a commercially available kit (DyLight Microscale Antibody Labeling Kits, Thermo Scientific).

Results

14-3-3 immunoreactivity in patients with FALS

In all the three FALS cases, LBHIs were observed inside the anterior horn cells (Figure 1A–C). All the LBHIs observed on H&E showed strong pan 14-3-3 immunoreactivity (Figure 1D–F). Using 14-3-3 isoform-specific antibodies, all the LBHIs detected by H&E (Figure 2A, B) were intensely immunopositive both for 14-3-3β (Figure 2C) and 14-3-3γ (Figure 2D).

Double immunofluorescent-stained sections showed that pan 14-3-3 was co-localized with SOD1 in the LBHI (Figure 3).

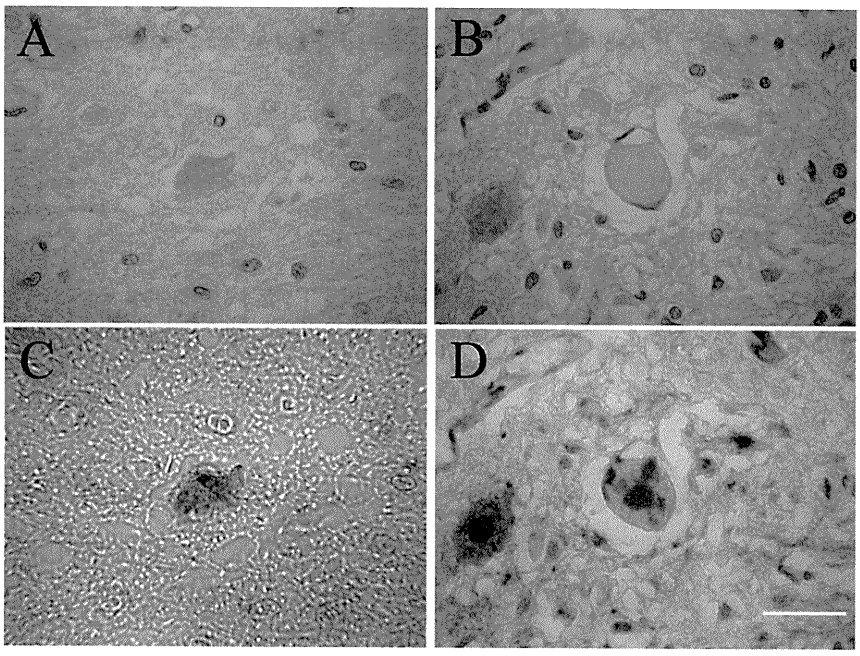

Figure 2. LBHIs immunopositive for 14-3-3β or 14-3-3γ in FALS patients. A and B are the same sections as C and D, respectively. The identical LBHIs observed on H&E (A, B) in the anterior horn cells are intensely immunostained with 14-3-3β (C) and 14-3-3γ (D). Bar indicates 50 μm.
doi:10.1371/journal.pone.0020427.g002

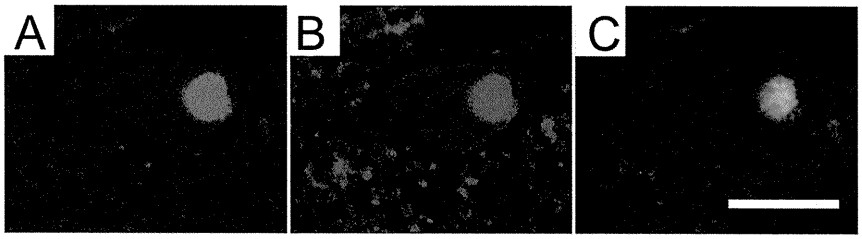

Figure 3. A LBHI double-positive for 14-3-3 and SOD1 in a FALS patient. A LBHI in an anterior horn cell is immunostained for pan 14-3-3 (A, green) and SOD1 (B, red), and the merged image is shown in C (yellow). Bar indicates 50 μm.
doi:10.1371/journal.pone.0020427.g003

Mutant SOD1 immunoreactivy in the mutant SOD1-Tg, the wild-type SOD1-Tg, and non-Tg wild-type mice

In mutant SOD1-Tg mice, C4F6 immunoreactivity was observed in the remaining anterior horn cells with cytoplasmic inclusions (Figure 4A). Immunoreactivity for C4F6 was restricted to the glial cells that were morphologically consistent with microglia in wild-type SOD1-Tg mice (Figure 4B) and absent in non-Tg wild-type mice (Figure 4C).

14-3-3 immunoreactivity in the mutant SOD1-Tg, the wild-type SOD1-Tg, and non-Tg wild-type mice

Pan 14-3-3, 14-3-3β and 14-3-3γ immunoreactivities were grossly different between the mutant SOD1-Tg and the wild-type SOD1-Tg or non-Tg wild-type mice (Figure 5).

Such 14-3-3 immunoreactivities were strong in most of the remaining anterior horn cells of the mutant SOD1-Tg mice (Figure 5A, D, G), although they were not observed in the wild-type SOD1-Tg (Figure 5B, E, H) or non-Tg wild-type mice (Figure 5C, F, I).

Double immunofluorescent staining of C4F6 and 14-3-3β or 14-3-3γ in SOD1-Tg mice

As described above, the strong immunoreactivity of 14-3-3β and 14-3-3γ were observed in the mutant SOD1-Tg mice but not in the wild-type SOD1-Tg mice. Wherein, the distribution of immunoreactivity for C4F6, 14-3-3β and 14-3-3γ was analyzed.

All the three immunoreactivities were observed in the neuronal somata of the anterior horn cells. Furthermore, double immunofluorescent staining showed that both 14-3-3β and 14-3-3γ were partially co-localized with C4F6 in mutant SOD1-Tg mice (Figure 6).

In negative immunohistochemical controls, some sections were incubated with the primary antibody (0.2 μg/ml) preabsorbed with an excess amount of the antigenic peptides, pan 14-3-3, 14-3-3β and 14-3-3γ (10 μg/ml). No specific immunopositive staining was detected in these control sections.

Other 14-3-3 isoforms in the mutant SOD1-Tg mice and the wild-type SOD1-Tg mice

Immunoreactivitiy for 14-3-3ε, η, θ, σ, and ζ was observed in the neuronal somata and processes in the spinal cord. However, there were no remarkable differences in the distribution or intensity of the immunoreactivities between the mutant SOD1-Tg and wild-type SOD1-Tg mice.

Discussion

In this study, LBHIs in all FALS cases showed intense pan 14-3-3, 14-3-3β and 14-3-3γ immunoreactivities. Furthermore, the double immunofluorescent study showed 14-3-3 proteins were co-localized with SOD1 in LBHIs. Such distribution patterns were quite similar to those of the mutant SOD1-Tg mice. This is the first report that demonstrates a close relationship between 14-3-3 and SOD1 both in patients with FALS and mutant SOD1-Tg mice.

We have previously reported the localization of 14-3-3 proteins in the ubiquitinated intraneuronal inclusions in the anterior horn cells from patients with sporadic ALS [12]. We also already reported 14-3-3 immunoreactivity in the LBHIs in the anterior horn cells from a patient with FALS, with a two-base pair deletion in the SOD1 gene [19]; however, the co-localization of SOD1 and 14-3-3 was not assessed. Therefore the role of 14-3-3 proteins in LBHI formation with a SOD1 mutation has remained unclear. The co-localization of 14-3-3 and SOD1 in the LBHIs in both FALS patients and mutant SOD1-Tg mice suggested that 14-3-3 may play an important role in the formation of SOD1-containing LBHIs. The similar 14-3-3 positivity in the LBHI of sporadic ALS and FALS with SOD1 mutation further suggests that 14-3-3 is involved in the pathogenesis of ALS, irrespective of whether it is sporadic or familial.

Among the various isoforms of 14-3-3 protein, Kaneko and Hachiya proposed the possibility that a distinctive function of 14-3-3ζ might be as a sweeper for misfolded proteins, such as aggregates or inclusion bodies [20]. Santpere et al. suggested that

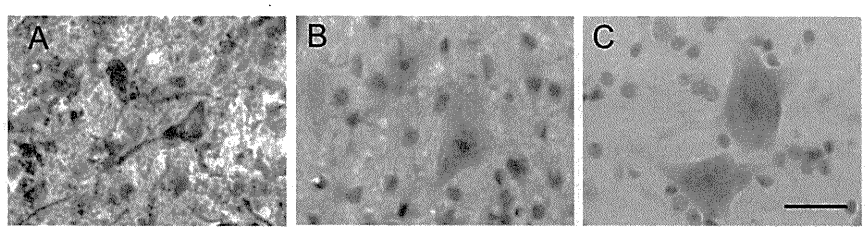

Figure 4. Neuronal inclusions immunopositive for C4F6 in mice. Strong immunoreactivity for C4F6 (A) was observed in the somatodendritic compartment with cytoplasmic inclusions in the mutant SOD1-Tg mice. Immunoreactivity for C4F6 was restricted to glial cells morphologically consistent with microglia in the wild-type SOD1-Tg mice (B) and absent in the non-Tg wild-type mice (C). Bar indicates 50 μm.
doi:10.1371/journal.pone.0020427.g004

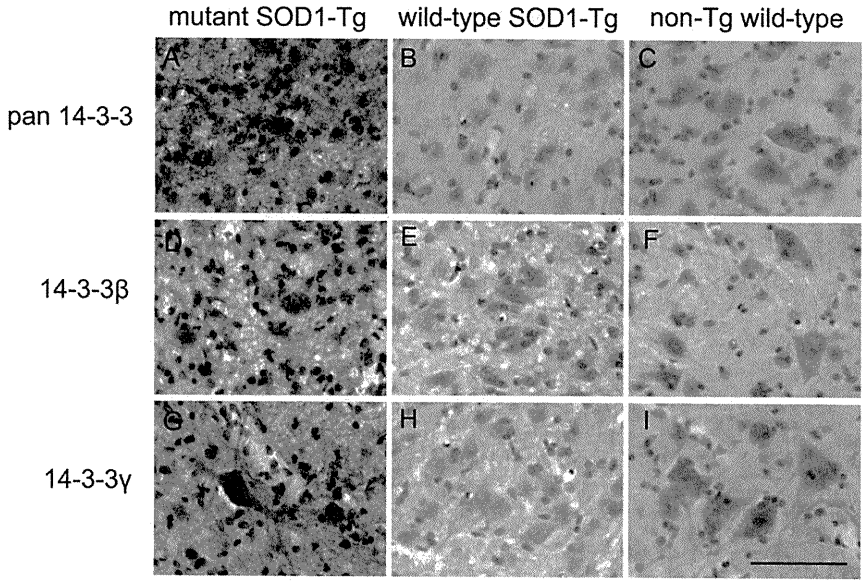

Figure 5. Neuronal inclusions immunopositive for pan 14-3-3, 14-3-3β, and 14-3-3γ in the spinal cord of SOD1-Tg mice. In mutant SOD1-Tg mice, strong immunoreactivity for pan 14-3-3 (A), 14-3-3β (D), and 14-3-3γ (G) were observed in the neuronal cytoplasm or neuronal process of the lumbar anterior horn cells. Such immunoreactivities were not observed in the wild-type SOD1-Tg (B, E, H) or non-Tg wild-type mice (C, F, I). Bar indicates 50 μm.
doi:10.1371/journal.pone.0020427.g005

the 14-3-3γ and 14-3-3ζ isoforms may be the targets of oxidative damage in Alzheimer's disease [21], and some neurofibrillary tangles were reported to be immunolabeled with 14-3-3β and 14-3-3γ [22]. Similarly, 14-3-3 proteins have been co-localized in Lewy bodies [23] and in glial cytoplasmic inclusions from patients with multiple system atrophy [24]. In our recent study, 14-3-3β and 14-3-3γ were strongly expressed in the neuronal somata and processes of anterior horn cells in the spinal cord of mutant human α-synuclein (A53T)-Tg mice, an animal model of Parkinson's disease (PD) [25]. Therefore, 14-3-3β and 14-3-3γ may be the key isoforms associated with the formation of α-synuclein- and SOD1-containing inclusions. This raises the possibility that there might be a common mechanism for inclusion formation at least between ALS and PD.

An insufficient function of the molecular chaperones may be directly involved in the loss of motor neurons in ALS [26,27]. Under non-pathological conditions, 14-3-3 proteins play important roles in signal transduction, apoptotic cell death and cell cycle

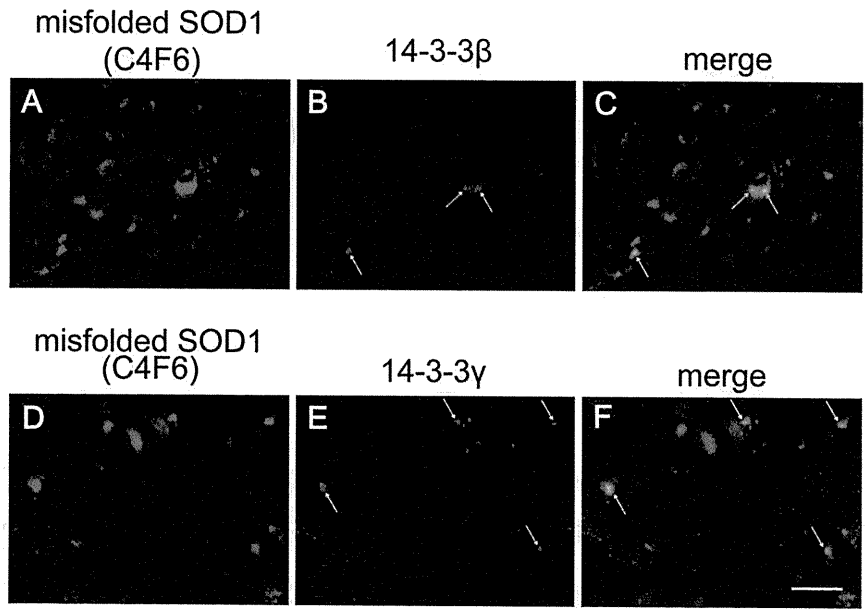

Figure 6. Neuronal inclusions double-positive for C4F6 and 14-3-3 in the spinal cord of mutant SOD1-Tg mice. Immunofluorescence for C4F6 (A, D, green), 14-3-3β (B, red), and 14-3-3γ (E, red), double immunofluorescence for C4F6 and 14-3-3β (C, merge), and double immunofluorescence for C4F6 and 14-3-3γ (F, merge) are shown in the anterior horn cells. Bar indicates 20 μm.
doi:10.1371/journal.pone.0020427.g006

control. 14-3-3 proteins inhibit apoptosis by binding to and inactivating pro-apoptotic proteins, including the mitochondrial Bcl-2 family member BAD, apoptosis signal-regulating kinase 1 (ASK1), and the Forkhead transcription factor FKHRL1 [10]. Therefore, the sequestration of 14-3-3 may cause neuronal dysfunction and thus contribute to cell death. Strong immunoreactivity for 14-3-3 in the LBHIs of FALS patients and in the mutant SOD1-Tg mice suggested that 14-3-3 proteins are trapped in the LBHIs, and this deficiency of the 14-3-3 proteins causes motor neuronal death in patient with FALS.

Acknowledgments

We would like to express our cordial gratitude to Ms. Hitomi Nakabayashi for her excellent technical assistance, and Dr. Ahmad Khundakar for his critical reading of the manuscript.

Author Contributions

Conceived and designed the experiments: MI HT HI SS RT. Performed the experiments: YO YS YK UM MO. Analyzed the data: YO MI. Contributed reagents/materials/analysis tools: SK HY AH. Wrote the paper: YO MI.

References

1. Byrne S, Walsh C, Lynch C, Bede P, Elamin M, et al. (2010) Rate of familial amyotrophic lateral sclerosis: a systematic review and meta-analysis. J Neurol Neurosurg Psychiatry.
2. Rosen DR, Siddique T, Patterson D, Figlewicz DA, Sapp P, et al. (1993) Mutations in Cu/Zn superoxide dismutase gene are associated with familial amyotrophic lateral sclerosis. Nature 362: 59–62.
3. Shibata N, Hirano A, Kobayashi M, Siddique T, Deng HX, et al. (1996) Intense superoxide dismutase-1 immunoreactivity in intracytoplasmic hyaline inclusions of familial amyotrophic lateral sclerosis with posterior column involvement. J Neuropathol Exp Neurol 55: 481–490.
4. Rothstein JD (2009) Current hypotheses for the underlying biology of amyotrophic lateral sclerosis. Ann Neurol 65 Suppl 1: S3–9.
5. Shibata N (2001) Transgenic mouse model for familial amyotrophic lateral sclerosis with superoxide dismutase-1 mutation. Neuropathology 21: 82–92.
6. Murayama S, Ookawa Y, Mori H, Nakano I, Ihara Y, et al. (1989) Immunocytochemical and ultrastructural study of Lewy body-like hyaline inclusions in familial amyotrophic lateral sclerosis. Acta Neuropathol 78: 143–152.
7. Mizusawa H, Matsumoto S, Yen SH, Hirano A, Rojas-Corona RR, et al. (1989) Focal accumulation of phosphorylated neurofilaments within anterior horn cell in familial amyotrophic lateral sclerosis. Acta Neuropathol 79: 37–43.
8. Casareno RL, Waggoner D, Gitlin JD (1998) The copper chaperone CCS directly interacts with copper/zinc superoxide dismutase. J Biol Chem 273: 23625–23628.
9. Boston PF, Jackson P, Thompson RJ (1982) Human 14-3-3 protein: radioimmunoassay, tissue distribution, and cerebrospinal fluid levels in patients with neurological disorders. J Neurochem 38: 1475–1482.
10. Fu H, Subramanian RR, Masters SC (2000) 14-3-3 proteins: structure, function, and regulation. Annu Rev Pharmacol Toxicol 40: 617–647.
11. Aitken A (1996) 14-3-3 and its possible role in co-ordinating multiple signalling pathways. Trends Cell Biol 6: 341–347.
12. Kawamoto Y, Akiguchi I, Nakamura S, Budka H (2004) 14-3-3 proteins in Lewy body-like hyaline inclusions in patients with sporadic amyotrophic lateral sclerosis. Acta Neuropathol 108: 531–537.
13. Malaspina A, Kaushik N, de Belleroche J (2000) A 14-3-3 mRNA is up-regulated in amyotrophic lateral sclerosis spinal cord. J Neurochem 75: 2511–2520.
14. Nakano I, Hirano A, Kurland LT (1984) Familial amyotrophic lateral sclerosis:Neuropathology of two brothers in American "C" family. Neurol Med(Tokyo) 20: 458–471.
15. Hirano A, Kurland LT, Sayre GP (1967) Familial amyotrophic lateral sclerosis. A subgroup characterized by posterior and spinocerebellar tract involvement and hyaline inclusions in the anterior horn cells. Arch Neurol 16: 232–243.
16. Gurney ME, Pu H, Chiu AY, Dal Canto MC, Polchow CY, et al. (1994) Motor neuron degeneration in mice that express a human Cu,Zn superoxide dismutase mutation. Science 264: 1772–1775.
17. Ceballos-Picot I, Nicole A, Briand P, Grimber G, Delacourte A, et al. (1991) Neuronal-specific expression of human copper-zinc superoxide dismutase gene in transgenic mice: animal model of gene dosage effects in Down's syndrome. Brain Res 552: 198–214.
18. Urushitani M, Ezzi SA, Julien JP (2007) Therapeutic effects of immunization with mutant superoxide dismutase in mice models of amyotrophic lateral sclerosis. Proc Natl Acad Sci U S A 104: 2495–2500.
19. Kawamoto Y, Akiguchi I, Fujimura H, Shirakashi Y, Honjo Y, et al. (2005) 14-3-3 proteins in Lewy body-like hyaline inclusions in a patient with familial amyotrophic lateral sclerosis with a two-base pair deletion in the Cu/Zn superoxide dismutase (SOD1) gene. Acta Neuropathol 110: 203–204.
20. Kaneko K, Hachiya NS (2006) The alternative role of 14-3-3 zeta as a sweeper of misfolded proteins in disease conditions. Med Hypotheses 67: 169–171.
21. Santpere G, Ferrer I (2009) Retracted: "Oxidative damage of 14-3-3 zeta and gamma isoforms in Alzheimer's disease and cerebral amyloid angiopathy" [Neuroscience 146 (2007) 1640–1651]. Neuroscience 161: 663.
22. Umahara T, Uchihara T, Tsuchiya K, Nakamura A, Iwamoto T, et al. (2004) 14-3-3 proteins and zeta isoform containing neurofibrillary tangles in patients with Alzheimer's disease. Acta Neuropathol 108: 279–286.
23. Berg D, Riess O, Bornemann A (2003) Specification of 14-3-3 proteins in Lewy bodies. Ann Neurol 54: 135.
24. Kawamoto Y, Akiguchi I, Nakamura S, Budka H (2002) Accumulation of 14-3-3 proteins in glial cytoplasmic inclusions in multiple system atrophy. Ann Neurol 52: 722–731.
25. Shirakashi Y, Kawamoto Y, Tomimoto H, Takahashi R, Ihara M (2006) alpha-Synuclein is colocalized with 14-3-3 and synphilin-1 in A53T transgenic mice. Acta Neuropathol 112: 681–689.
26. Bruening W, Roy J, Giasson B, Figlewicz DA, Mushynski WE, et al. (1999) Up-regulation of protein chaperones preserves viability of cells expressing toxic Cu/Zn-superoxide dismutase mutants associated with amyotrophic lateral sclerosis. J Neurochem 72: 693–699.
27. Yamashita H, Kawamata J, Okawa K, Kanki R, Nakamizo T, et al. (2007) Heat-shock protein 105 interacts with and suppresses aggregation of mutant Cu/Zn superoxide dismutase: clues to a possible strategy for treating ALS. J Neurochem 102: 1497–1505.

ALS-SOD1 の臨床と病理

青木正志　加藤信介

SOD1 遺伝子異常に伴う家族性 ALS(ALS1)

家族性 ALS の原因遺伝子が発見されて以来，世界各国の研究室から 100 種類を超える SOD1 遺伝子変異が報告されている[1~4]．その多くの症例は，家族歴を除けば臨床的には孤発性 ALS との区別ができない．さらには，一見孤発性に見えても SOD1 遺伝子変異が同定されることもある．この SOD1 遺伝子変異が家族性 ALS 症例全体のどのくらいの割合で存在するかは議論の多いところであるが，米国では 20%程度とされてきた．一方，筆者らを含む日本のグループでも多くの SOD1 変異を報告してきたが，未だにわが国にどのくらいの頻度で ALS1 の患者が存在するかのデータはない．

東北大学ではこれまでに，常染色体優性遺伝形式が疑われる日本人の家族性 ALS 91 家系の解析を行い，その 22%にあたる 20 家系において遺伝子変異(いずれも点突然変異)を同定している(図 1)．これらの解析により，従来から家族性 ALS 一般に指摘されてきたことではあるが，孤発性 ALS に比較して ALS1 では下肢からの発症が多いことが確認された．また，必ずしも上位運動ニューロン徴候を伴わない症例の存在も確認されている．

SOD1 遺伝子変異による臨床像の違い

同じ SOD1 遺伝子の異常であっても，各点突然変異によりその臨床像にはかなりの違いが認められる．東北大学神経内科の症例における SOD1 変異と罹病期間の関係を図 2 に示す．すなわち，SOD1 変異の種類により ALS1 の発症後の経過は全く異なるが，各点突然変異によりおよその罹

あおき まさし　東北大学大学院教授/医学系研究科神経内科
かとう しんすけ　鳥取大学准教授/脳神経医科学講座脳病態医科学分野

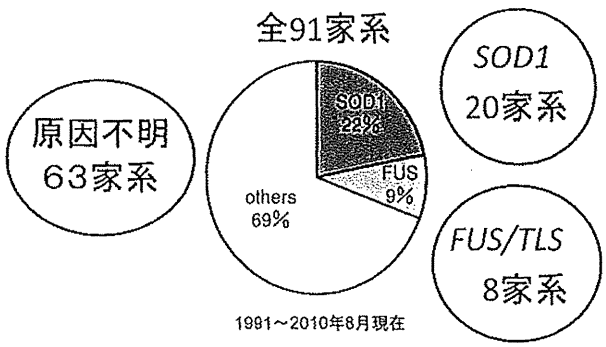

図 1　東北大学神経内科における家族性 ALS の遺伝子解析
常染色体優性遺伝形式が疑われる日本人の家族性 ALS 91 家系の解析を行い，その 22%にあたる 20 家系において遺伝子変異(いずれも点突然変異)を同定している．

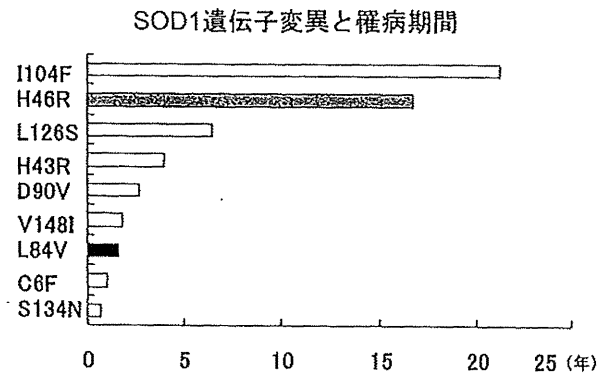

図 2　ALS1 症例おける SOD1 変異と臨床経過
東北大学神経内科の症例における SOD1 遺伝子変異と罹病期間の関係を示す．東北大学では L84V および H46R 変異を導入したトランスジェニックマウスの作成を行い，同マウスにおいても L84V 変異を伴うものと比較して，H46R 変異を伴うものは発症から死亡までの罹病期間が長いことを確認している．

0289-0585/11/¥500/論文/JCOPY

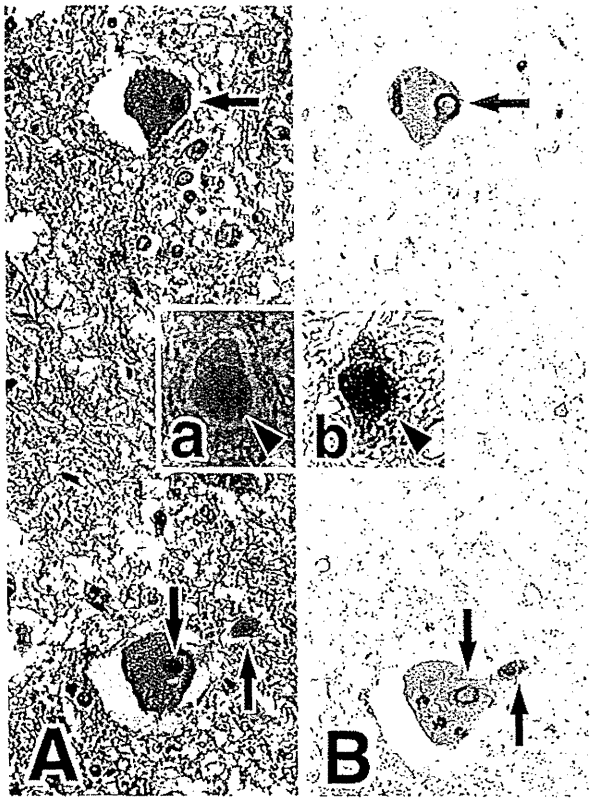

図 3　LBHI(A, B)と Ast-HI(a, b)の光顕像
A, a) HE 染色. B, b) SOD1 染色. 脊髄前角細胞内に LBHI(矢印)が認められる(A). LBHI は強い SOD1 陽性を示す(B). 同様に, Ast-HI(a, 矢頭)も SOD1 陽性を示す(b, 矢頭).

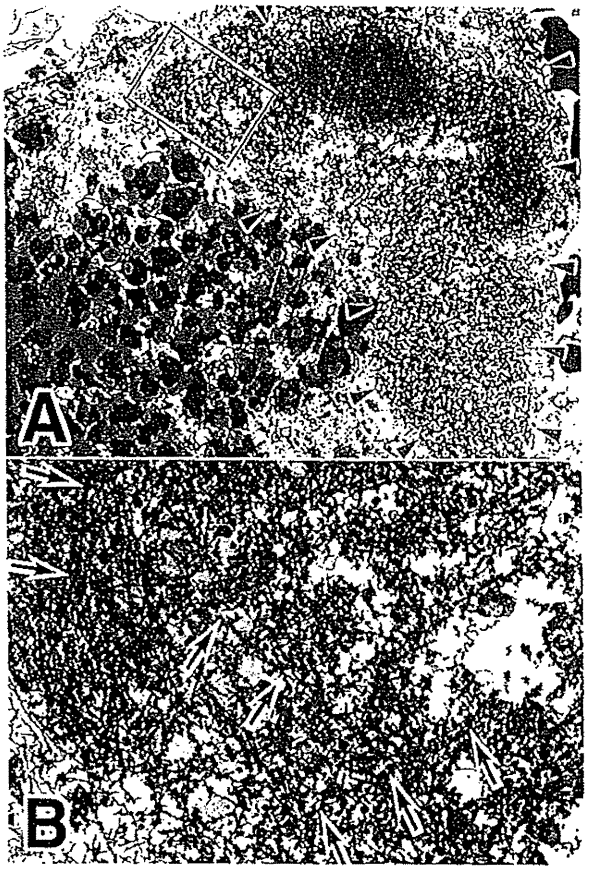

図 4　脊髄前角細胞内 LBHI の超微形態像
A) LBHI の弱拡大像(矢頭). 異常線維が密に存在している部位が core に, 粗になっている周辺部位が halo に相当する. B) LBHI(A の矩形部位)の強拡大像. LBHI の本体である granule-coated fibril は矢印で示している.

病期間が決まっている.

SOD1 遺伝子変異と浸透率

ある病気の原因遺伝子に変異を持っていても生涯にわたり健康で, その病気を発症しないヒトの存在も知られており, ある遺伝子型の個体がある表現型をとる確率を浸透率とよんでいる. SOD1 変異の浸透率はその各々の変異により異なると考えられており, H46R 変異はほぼ 100%と考えられる(遺伝子異常があればほぼ間違いなく発症する)[2]. 一方, 浸透率の低い変異の家系では一見孤発例のようにみえることがある. L126S 変異は浸透率の低い変異と考えられているが, この変異がホモ接合体となると, ヘテロ接合体と考えられる家系内の他の症例と比較して, 発症の若年化および臨床型の重症化がみられる[4].

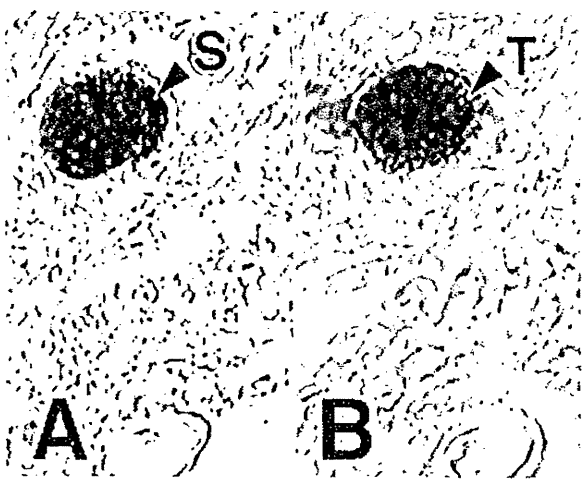

図 5　C111Y 変異を伴う ALS1 における LBHI
C111Y-ALS1 における LBHI は, SOD1(A：矢頭と S)と TDP-43(B：矢頭と T)の両者に陽性を示している.

ALS1の基本病理像

ALS1の病理像は孤発性の古典的ALS(sporadic ALS：SALS)の病理像が基本であり，この基本病理像にALS1としての特徴的病理像が積み重なることにより，ALS1の神経病理像が形成される．

ALS1の病理像は上位および下位運動神経系が障害されることが基本である．しかし，ALS1の上位運動神経系の病変はSALSに比べてごく軽度であることが特徴であり，病変の主体は下位運動神経系である[1,2]．時には上位運動神経系の病変が全く目立たないこともある．ただし，長期生存例においては上位運動神経系の障害も顕著となる．すなわち，動眼・滑車・外転の各神経核とOnufrowicz核以外の脳神経運動核と脊髄前角運動細胞(α-motoneuron)の変性・消失が主体である．脊髄前角細胞が変性・消失すれば，再構築機転としての反応性astrocyteの増殖とともに，前角・前根が萎縮し前角内有髄線維は減少する．

ALS1の特徴的病理像

基本病理像に加えてALS1の特徴的病理像としては，① 後索中間根帯の変性，② Clarke柱neuronと後脊髄小脳路(Clarke柱neuronの軸索路)の変性，③ 神経細胞内Lewy小体様硝子様封入体(neuronal Lewy-body-like hyaline inclusion：LBHI)とアストロサイト内硝子様封入体(astrocytic hyaline inclusion：Ast-HI)の存在，④ Buninabodyが観察されない，以上4項目と考えている[5,6]．① 腰髄では薄束，頸髄では楔状束(いわゆるFlechsigの中間根帯)が淡明化する．病変が高度になると後索中央部全体が変性を呈する．② Clarke柱neuronの変性・脱落に伴い，これらneuronの軸索路である後脊髄小脳路の変性を惹起する．病変が高度になると前脊髄小脳路も障害される．④ Buninabodyに関しては，ロシアの女性病理学者T.L. Buninaが2家系2症例の家族性ALS症例においてその存在を報告したが[6]，それらの症例はSOD1変異を伴わない家族性ALS症例であったと筆者らは想像している．

Neuronal LBHIとAst-HI

Neuronal LBHIとAst-HIについては，1967年にHiranoらによりneuronal LBHIが，1996年に著者らによりAst-HIが，ALS1の特徴的所見として記載された[5,6]．Neuronal LBHIは光顕的にヘマトキシリン・エオジン(HE)染色でeosinophilic coreと淡いhaloよりなり，あたかもパーキンソン病のLewy小体のように見えるところにその名の由来がある(図3A)．光顕上内部は無構造で均一であるためhyaline(硝子)という表現がなされている．Ast-HIについては，HE染色ではneuronal LBHIとほぼ同一構造を呈し，eosinophilicで均質無構造な硝子様を呈している．多くは円形から楕円形であり(図3a)，時にeosinophilic coreと淡いhaloを認めることがある．

Neuronal LBHIとAst-HIはともに免疫組織化学的にSOD1に強陽性を示す(図3B, b)[5,6]．両封入体は野生型と変異型の両者のSOD1 epitopeを有している[6]．超微形態的には，neuronal LBHIもAst-HIもともに約15～25 nm径のgranule-coated fibrilと顆粒状構造物(granular material)からなっている(図4)．このgranule-coated fibrilの横断面は管状構造をなしておらず，顆粒稠密状を呈している．その形成過程については，変異SOD1をcore proteinの一つとして凝集し，野生型SOD1や細胞内正常構成蛋白質をも取り込みながら，電顕的にはgranular materialが線維状に凝集し，granule-coated fibrilが形成されてくる超微形態的形成像が観察されている[6]．

すなわち，光顕的にSOD1陽性のLBHI/Ast-HIを同定するか，あるいは超微形態的に約15～25 nm径のgranule-coated fibrilを同定すれば，その生体系には変異SOD1遺伝子異常が存在しているといっても過言ではないと筆者らは考えている．

SOD1とTAR DNA binding protein 43(TDP-43)

一般的に，SALS・変異SOD1非関連家族性ALS・運動ニューロン疾患を伴う前頭側頭葉変性症frontotemporal lobar degeneration with motor neuron disease〔FTLD-

MND：terminology 上は，認知症を伴う ALS(ALS with dementia：ALSD と同一)]において出現する特徴的病理学的所見であるスケイン様封入体 skein-like inclusion(SLI)や球状封入体 round inclusion(RI)/spherical inclusion(SI)は TDP-43 陽性を呈するが，ALS1 の特徴的病理学的所見である LBHI や Ast-HI は TDP-43 陰性である．一方，LBHI/Ast-HI は SOD1 陽性であるが，SLI/RI/SI は SOD1 陰性を示す．これらの SOD1 と TDP-43 の病理学的所見は，変異 SOD1 に関連しない運動神経細胞死には TDP-43 が関与し(TDP-43 proteinopathy)，変異 SOD1 に関連する運動神経細胞死(mutant SOD1 proteinopathy)には TDP-43 が本質的には関与していないという仮説が直感的に成立しそうな感を与える．しかし，C111Y 変異 SOD1 を伴う ALS1(C111Y-ALS1)においては，SOD1 と TDP-43 の両者陽性の LBHI が多数存在している事実(図 5)[7]に加え，LBHI と SLI とが共存している H48Q-ALS1[5,6]や SLI を認める E100G-ALS1 の存在[5,6]は，運動神経細胞死の病態解明の病理学的糸口さえ単純に発見できるものではないと筆者らに語っているように思われる．

I113T 変異を伴う ALS1

I113T-ALS1 は LBHI/Ast-HI は存在せず，neurofilamentous conglomerate inclusion(NFCI)を高率に有する特徴がある[5,6]．NFCI は HE 染色ではごくわずかに好酸性を呈する均一な球状，または分葉状構造物である．免疫組織化学的にはリン酸化 neurofilament に強陽性を呈する．Ubiquitin には多くの NFCI は陰性を呈するが，NFCI の内部の一部には ubiquitin 陽性構造物を認めることもある．超微形態的には，NFCI は neurofilament の束が三次元的に糸巻き・渦巻きを形成して球状構造をしている．NFCI は SALS(5%以下)でも観察される．

謝辞： 本研究の一部は，文部科学省科学研究費補助金(No. S0801035)(SK)および厚生労働科学研究費補助金難治性疾患克服対策研究事業(MA，SK)の助成により行った．

文 献

1) Rosen DR, Siddique T, Patterson D, et al. Mutations in Cu/Zn superoxide dismutase gene are associated with familial amyotrophic lateral sclerosis. Nature. 1993；362：59-62.
2) Aoki M, Ogasawara M, Matsubara Y, et al. Mild ALS in Japan associated with novel SOD mutation. Nat Genet. 1993；5：323-4. [erratum：Nat Genet. 1994；6：225.]
3) Andersen PM, Sims KB, Xin WW, et al. Sixteen novel mutations in the Cu/Zn superoxide dismutase gene in amyotrophic lateral sclerosis：a decade of discoveries, defects and disputes. Amyotroph Lateral Scler Other Motor Neuron Disord. 2003；4：62-73.
4) Kato M, Aoki M, Ohta M, et al. Marked reduction of the Cu/Zn superoxide dismutase polypeptide in a case of familial amyotrophic lateral sclerosis with the homozygous mutation. Neurosci Lett. 2001；312：165-8.
5) Kato S, Shaw P, Wood-Allum C, et al. Amyotrophic lateral sclerosis. In：Dickson D, editor. Neurodegeneration：the molecular pathology of dementia and movement disorders. Basel：ISN Neuropath Press；2003. p. 350-68.
6) Kato S. Amyotrophic lateral sclerosis models and human neuropathology：similarities and differences. Acta Neuropathol. 2008；115：97-114.
7) Sumi H, Kato S, Mochimaru Y, et al. Nuclear TAR DNA binding protein 43 expression in spinal cord neurons correlates with the clinical course in amyotrophic lateral sclerosis. J Neuropathol Exp Neurol. 2009；68：37-47.

EXTRA
Dementia
and Geriatric
Cognitive Disorders

Dement Geriatr Cogn Disord Extra 2012;2:190–199
DOI: 10.1159/000338244
Published online: April 24, 2012

Original Research Article

Prevalence of Dementia and Mild Cognitive Impairment in the Rural Island Town of Ama-cho, Japan

Kenji Wada-Isoe[a] Yusuke Uemura[a] Satoko Nakashita[a]
Mika Yamawaki[a] Kenichiro Tanaka[a] Mikie Yamamoto[a]
Hiroshi Shimokata[b] Kenji Nakashima[a]

[a]Division of Neurology, Department of Brain and Neurosciences, Faculty of Medicine, Tottori University, Yonago, and [b]Department of Epidemiology, National Center for Geriatrics and Gerontology, Obu, Japan

Key Words
Alzheimer's disease · Vascular dementia · Dementia with Lewy bodies · Mild cognitive impairment · Epidemiology

Abstract
Aims: In order to determine the prevalence of dementia and mild cognitive impairment (MCI), we conducted a population-based study in Japan. ***Methods:*** Participants included 924 subjects aged 65 years or older who resided in the town of Ama-cho. In phase 1 of the study, the Mini-Mental State Examination and Clinical Dementia Rating were administered for screening purposes. In phase 2 of the study, the subjects who screened positive were further examined by neurologists. Dementia and MCI were diagnosed by means of DSM-IV and International Working Group on MCI criteria, respectively. ***Results:*** By the prevalence date of June 1, 2010, 24 subjects had deceased or lived outside the town. In total, 723 of the remaining 900 subjects received a phase 1 test. In phase 2, 98 subjects were diagnosed with amnestic MCI, 113 subjects with non-amnestic MCI, and 82 subjects with dementia. Of the subjects who did not receive the phase 1 test, 66 subjects were diagnosed as having dementia according to data from their town medical card or the Long-term Care Insurance System. The crude prevalence of amnestic MCI, non-amnestic MCI, and dementia were 10.9, 12.6, and 16.4%, respectively. ***Conclusion:*** Consistent with the striking increase in the number of elderly individuals, we report higher prevalence of MCI and dementia in Japan than previously described.

Kenji Wada-Isoe

Department of Neurology, Institute of Neurological Sciences
Faculty of Medicine, Tottori University
36-1 Nishi-cho, Yonago 683-8504 (Japan)
Tel. +81 85 938 6757, E-Mail kewada@med.tottori-u.ac.jp